ABSTRACT

ROJAS, CARLYE RIMMELE. Controlled Particle Transport in a Human Airway Replica. (Under the direction of William L. Roberts).

The goal of this research is a proof-of-concept for targeted aerosol delivery and validation of computational results. Sodium chloride particles, with a monodisperse particle size of one micrometer are used to represent a drug aerosol in the experimental validation of computational results. A complex oral airway, including a mouth, larynx, pharynx, and trachea was constructed out of laser cured resin, using a three-dimensional printing method. A symmetric three generation (G0 to G3) bifurcating bronchial airway was constructed using the same process. Two-phase flow was conducted through these models to yield particle transport results. The bulk air flow was 2 liters per minute, the highest observed flow rate that will allow the flow to remain laminar throughout the airway model. The flow rate of the particle seeded flow was maintained at 20 milliliters per minute. The velocities of these two flow rates remain within an order of magnitude of each other to inhibit vortices created by shear forces when the two flows were introduced. A series of nozzles (constructed using SL) were used to control the particle injection location. A one millimeter inner diameter seed nozzle is offset, from the center, a given percent of the radius. There were five nozzles, with increasingly offset seed tubes, 0% (centerline of axisymmetric nozzle), 20%, 40%, 60%, and 80%. The airway model was attached to the nozzle so that the nozzle exit is in the same plane as the mouth entrance. The nozzle was rotated so that the seed tube exit can be positioned at various angles within the circular cross-section. By controlling the particle release position, the deposition efficiency can be increased, dramatically, as compared to the uniform

injection of the drug. The results show the controlled particle release can determine which branch or branches of the third generation bifurcating bronchial airway the particles will exit. While numerous previous researchers have studied the deposition effects of a uniform injection of aerosol particles in the human airways, the controlled position of particle release is an original idea.

Controlled Particle Transport in a Human Airway Replica

by

Carlye Rimmele Rojas

A thesis submitted to the Graduate Faculty of
North Carolina State University
in partial fulfillment of the
requirements for the Degree of
Master of Science

Mechanical Engineering

Raleigh, North Carolina

2007

APPROVED BY:

_____

Dr. William L. Roberts
Chair of Advisory Committee

_____

Dr. Stefan Seelecke
Committee Member

_____

Dr. Clement Kleinstreuer
Committee Member

BIOGRAPHY

The author was born Carlye Jean Rimmele on October 9, 1981 in Flemington NJ, daughter of Jack and Kathy Rimmele and sister to older brother Zachary John, and younger brothers Ryan John and Schuylar John Rimmele. She is married to Cristian Rojas. After moving around the east coast Carlye's family moved to Cary, NC in 1997. Carlye attended and graduated from St. Mary's School in Raleigh. Carlye decided to attend North Carolina State University to remain close to her family. Upon completion of her Bachelors of Science in Aerospace Engineering in May 2003 Carlye decided to take a break from engineering and continue her job as a swim coach. In the summer of 2005 she went back to continue her education at North Carolina State University in pursuit of a Master of Science degree in Mechanical Engineering. She received a grant from the National Institute of Health under the direction of Dr. William L. Roberts. After completion of her Masters degree she will continue work on the current project with Dr. Chong Kim at the Environmental Protection Agency – Human Studies Division. Her ultimate life goal is to remain at home taking care of a house full of children.

TABLE OF CONTENTS

LIST OF TABLES

LIST OF FIGURES

1.0 Introduction

Inhalation of aerosol drugs is used extensively for treatment of respiratory system ailments. Recently the success of this methodology for the treatment of other diseases and rapid pain management has been researched. Current devices used for aerosol drug delivery have limited deposition efficiencies of 5 to 20% (Kleinstreuer et al., 2003). Since these aerosol drugs are sometimes aggressive and can harm healthy tissue, there is a need for an aerosol drug delivery system that has higher deposition efficiency. The innovative idea of injecting a small particle stream into only a small fraction of the airway inlet, and therefore controlling where particles deposit, was proposed. The proposed system revolves around a Smart Inhaler which will be able to control the particle release position, breathing pattern, and particle release time during the inhalation. Along with controlled particle release position, the other two key factors are: determining optimal aerosol characteristics (e.g. size, shape, and density) and controlling the waveform of the inhalation flow.

1.1. Common Drug Aerosol Inhalers

The pressurized metered dose inhaler (pMDI) has been the most commonly used device for drug aerosol delivery for over 40 years. The general operation of a pMDI begins with a pressurized container housing the aerosol. A propellant ejects the aerosol through a nozzle to create a spray which is then inhaled by the patient. This device has several systematic disadvantages which may lead to its decreased use (Keller et al., 1999). Successful operation relies on the patient's ability to synchronize the actuation of

the device with the inspiration of breath. These inhalers also have low deposition efficiency and high aerosol velocity.

Several devices currently being developed and used have a more promising future than the outdated pMDI. Deep lung penetration is enabled by the use of nebulizers, which deliver drugs in the form of small droplets or a mist. The current research regarding nebulizers focuses on developing portable units. Another series of devices uses a dry powder as the inhalant. These dry powder inhalers (DPI) are either passive or active. Passive DPIs rely on the inhaled air to generate particle entrainment and breakup of powder. Active DPIs have stored energy in the form of blister pack that assist in dispersing the drug powder (Dunbar et al., 1998). The latest pursuits in inhaler formulation and design are discussed in Crowder et al. (2001). The advancements in the mechanisms of nebulizers, pMDIs, and DPIs are discussed by Finlay et al. (2001). A thorough patent search has proved that the proposed Smart Inhaler is original in design and theory.

1.2. Smart Inhaler

The Smart Inhaler tube (also referred to as a nozzle) will enable the use of two separate flows. A bulk flow will flow through the majority of the nozzle, whereas a separate and significantly smaller tube will carry the particle flow into the mouth inlet. In order to control particle injection position the particle nozzle will be deflected and realigned by some actuating force. Due to severe space restrictions in the inhaler tube, an innovative method of introducing actuating forces to the system needed to be used.

Shape memory alloy (SMA) wires have two desirable qualities; pseudo-elasticity and shape memory effect. Pseudo-elasticity is the ability of the alloy to return to the original shape, after substantial deformation, by simple unloading. Shape memory effect refers to the alloy returning to the original shape by heating. By applying an electric current, the wire undergoes a hysteretic phase transformation between austenite and martensite or between twin phases of martensite depending on the temperature (Figure 1-1).

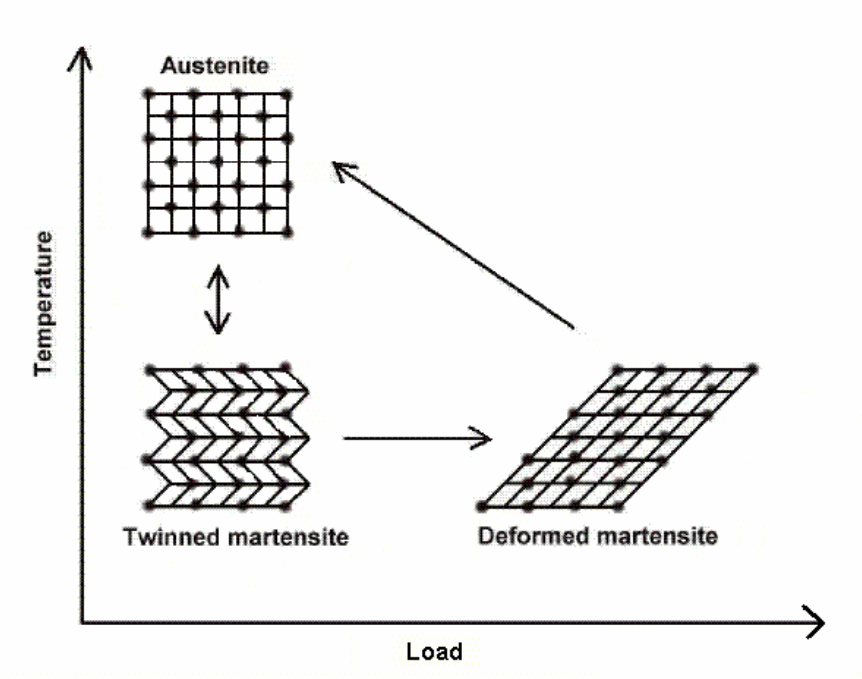

Figure 1-1: Phase transformation from the austenite to the martensite phase and twinned martensite to deformed martensite and back to austenite (Oulu University)

As the temperature is lowered, the high-temperature austenitic structure transforms into the twinned structure called martensite. The martensitic structure is easily deformed by

loading into the deformed martensite phase. Applying heat causes the deformed martensite to resume the austenitic form.

The design concept projects three sets of SMA wires will perform different operations. The first set (SMA 1) will be used to deflect the particle flow nozzle. The second set (SMA 2) will axially align the tip of the particle flow nozzle with the bulk airflow. The particle nozzle will need to be constructed out of a flexible material in order to achieve deflection and re-alignment. The third set of SMA wires (SMA 3) is projected to control the inlet air by moving the perforated sleeve with respect to the outer shell of the inhaler nozzle. Figure 1-2 illustrates the design concept. Some alterations in this design are expected.

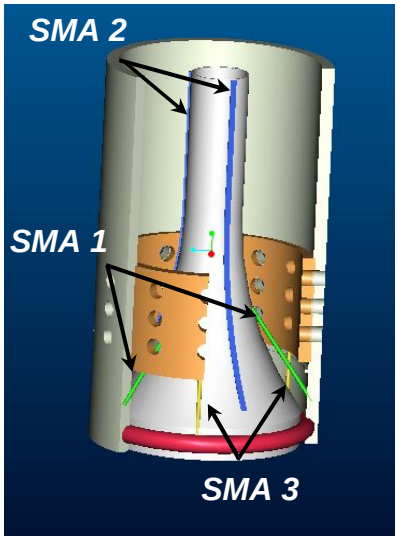

Figure 1-2: 3D model of SMA-actuated smart inhaler nozzle

Extensive work will be needed to design and construct the SMA nozzle. Geometry, material characteristics, and optimal actuator placement will require numerous

simulations. This endeavor will be executed by other members of the current research group.

1.3. Computational Fluid-Particle Dynamics

A significant amount of computational work has been done to investigate the success of targeted drug delivery. The methodology for controlled particle injection of drug delivery has been researched by Kleinstreuer and Zhang (2003b). Kleinstreuer and Zhang have done extensive work with laminar-to-turbulent flow regimes and micro- and nano-particles. Using a computer simulation model, they have observed an increase in aerosol drug deposition when the particle release position is controlled. The geometry used for the computational model consists of an oral cavity, pharynx, larynx and trachea, and a symmetric, planar, bronchial bifurcation (Figure 1-3).

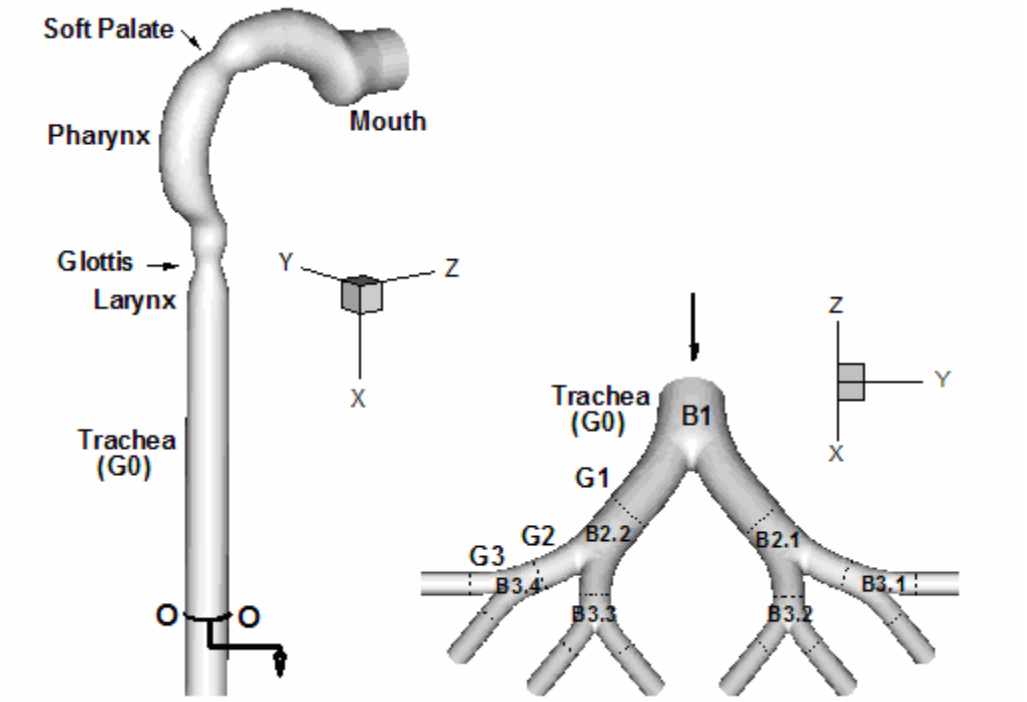

Figure 1-3: Geometry of the oral airway and bifurcations used for computational simulations (Zhang et al., 2004)

The oral airway is based on geometry reported by Cheng et al. (1999). The bifurcating model representing generations G0 (referring to the trachea) to G3 is adapted from Weibel (1963). The airflow was modeled using the low-Reynolds-number (LRN) k-ω model adapted from Wilcox (1993). Using the computational configuration and a controlled particle stream, deposition in targeted areas was investigated. The targeted area receives between 45 and 92% of the delivered aerosol (Kleinstreuer et al. 2003b).

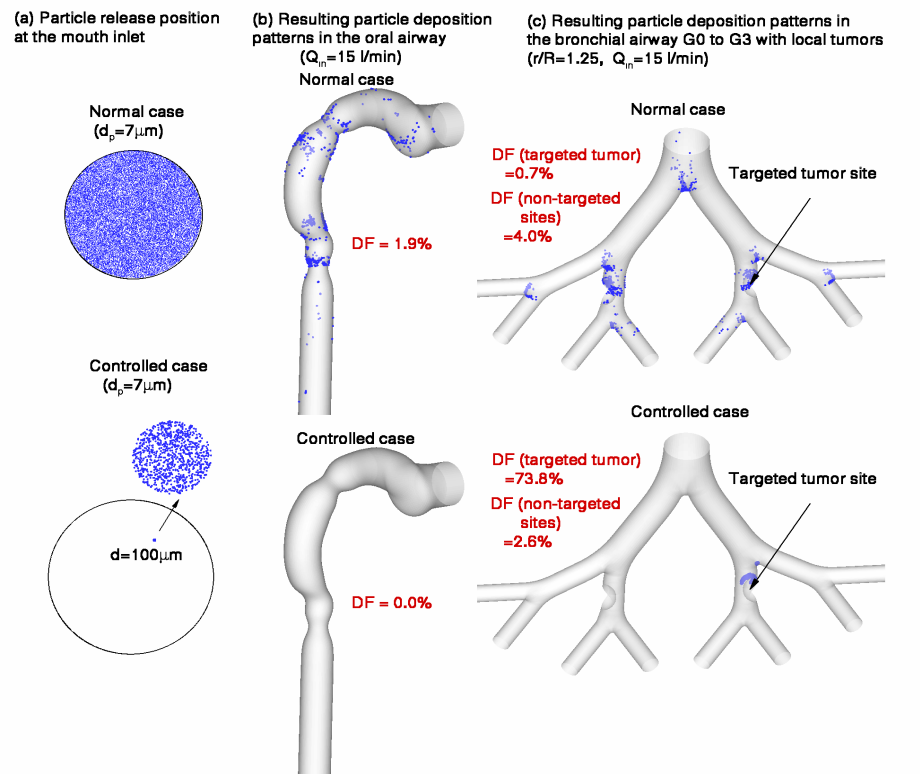

Figure 1-4: Computational models comparing the aerosol deposition factors of the uniform particle release case and the controlled case (Kleinstreuer and Zhang, 2003c)

Figure 1-4 shows the targeted sites as a tumor in the second generation of bifurcation. In this case the deposition efficiency increases from 0.7 % to almost 74%. This increase in aerosol deposition efficiency will not only help respiratory therapies; an amalgam of other treatments can also be aided by this increase such as pain management, growth hormones, diabetic therapy, cystic fibrosis therapy and much more. Targeted aerosol drug delivery is novel methodology with highly beneficial possibilities.

1.4. Current Research Focus

The primary aim of this part of the research was to validate the computational results of the targeted flow through the human oral and bronchial airways. Along with the control of the particle release position, achieved by the proposed smart inhaler, it is important to investigate the best particle characteristics and determine an optimal inhalation waveform.

The first step was construction of an accurate model of the human oral and bronchial airways. The proposed structure consisted of a modular form where each cross-section could be removed to study the flow at any point along the airway. The geometry of the oral airway, like the computational model, is based on actual casts of human airways (Cheng et al., 1999). The first upper bronchial airway model will be symmetric and planar. The dimensions and geometry of this model are based on the Weibel distribution (1963). A second, more realistic upper bronchial airway model is proposed. This model will have a fully three-dimensional, out-of-plane, asymmetric design. This asymmetric bifurcating model will be a significant to generating results as realistic as possible.

The second step was the design of a flow control apparatus including a mechanism that could control the flow rate through the model so that it is representative of an actual human inspiratory flow. The flow rates will be controlled by mass flow meters. Between the flow meters and the airway models, the air will be directed into a reservoir. A mechanism to create a breathing pattern will be mounted onto the sides of the reservoir. The boundary oscillation created by these mechanisms will cause a

variation in the rate of the flow enter the mouth inlet of the airway models. This oscillation superimposed on the flow has been shown to affect particle deposition (Finlay and Gehmlich, 2000).

The third step was the most extensive; the exploration for a seeding method and material that was representative of aerosol drugs, but would also fit the constraints of the research. The computational research has encompassed multiple particle size ranges and characteristics. Although all real drug aerosols are polydisperse, it is better to use monodisperse particles for research. By using particles of known characteristics it is easier to study the effect these characteristics have on the transport of the particles through the airways. Understanding the behavior of monodisperse particles throughout the mouth, larynx, pharynx, trachea, and into the lung will help determine the transport and deposition of aerosol drugs.

A data acquisition method that would go along with the particle seeding parameters was also investigated. The use of an argon-ion laser to perform Mie scattering is projected. The Mie scattering method requires the particles that scatter the light to be larger than the laser light wavelength. A camera can be used to acquire images of the light scatter off the particles.

The sister project within this research is the designing and building of nozzle that will hopefully meet the need of a more advanced aerosol drug delivery system. Although the nozzle design is a separate project, the experimental testing of these nozzles coincided with the experimental validation of the computational work.

2.0 Experimental Apparatus and Methods

Little previous work had been done for the experimental portion of this research. Other than drawings for the oral airway design and a rough model of the lung box, everything for this endeavor is original to this effort.

2.1. Lung Replica

The lung replica acted as a reservoir for the bulk air and as a mechanism for creating a breathing pattern. The replica was positioned directly upstream of the airway models. The reservoir aided the uniformity of the bulk flow entering the test section in constant flow rate cases. To create to transient flow, a mechanism was mounted to the sides of the lung replica. This mechanism changed the boundary of the reservoir forcing oscillations on the bulk flow, creating an inspiratory breathing pattern. The flow into the replica was always constant.

2.1.1. Plexiglas Box

A Plexiglas box with speakers was the existing design, built by Elizabeth Chatham. After testing the speakers it was determined these would not be sufficient for the breathing pattern needed for testing. However, the Plexiglas box was reserved for use with a new breathing pattern simulation system.

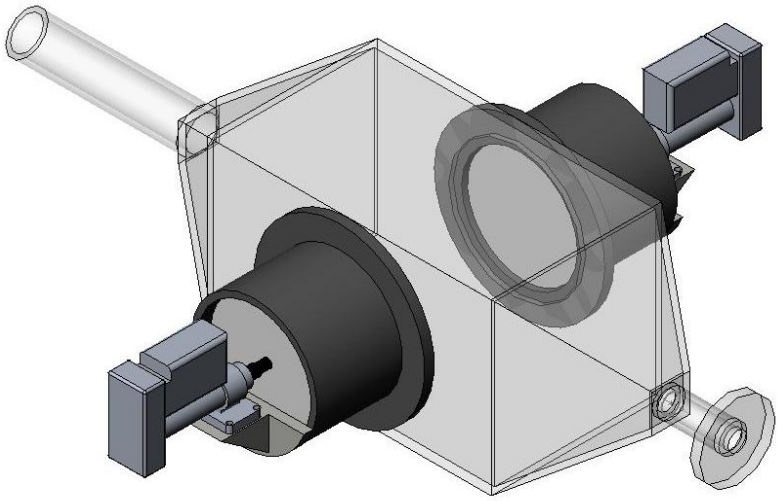

Figure 2-1: Plexiglas box used as lung replica

This lung box (Figure 2-1) was used for a majority of experiments run at the Applied Energy Research Laboratory (AERL), for this research. The bulk flow enters the rear of the box (tube shaped portion without flange). An L-shaped tube apparatus is inserted into the top of the box, this is the means of introducing the particle flow. The L-shaped apparatus can be seen in Figure 2-2.

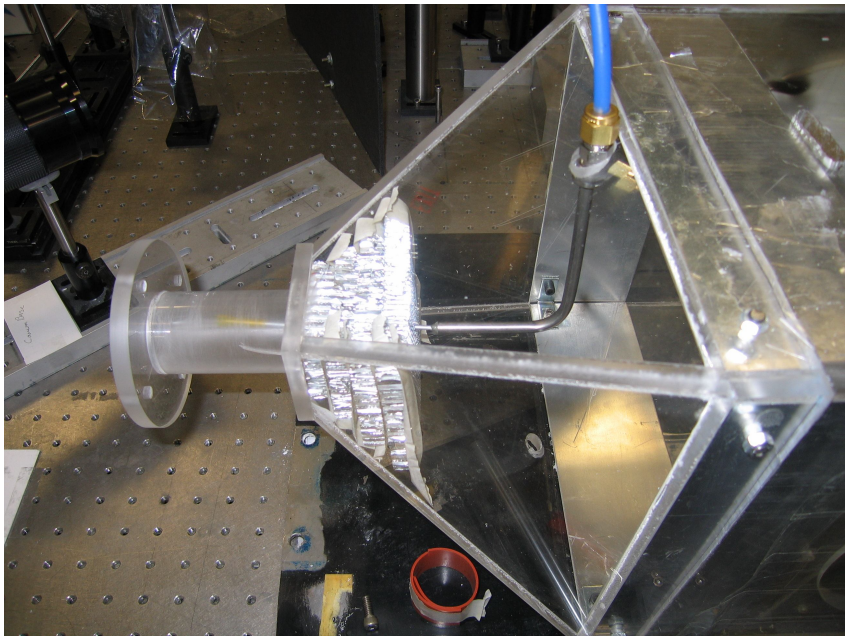

Figure 2-2: Front end of lung box with L-shaped seed tube apparatus

It was important to maintain a low profile in the design of the seed tube apparatus, to reduce interruptions in the bulk flow. A 0.635 cm diameter stainless steel tube is used to provide a rigid arm for the rest of the seed tube. Just before the seed tube goes through the aluminum honeycomb there is a transition to a 0.3175 cm diameter aluminum tube. A small diameter tube was needed to keep the low profile requirement. In early experiments the aluminum tube injected the seed flow directly into test section.

The four sheets of aluminum flow straightener seen in Figure 2-2 are a later generation of flow straightener arrangement. Flow straighteners are necessary to further reduce interruptions in the flow. The first iteration of flow straightener was three 3.81 cm round resin coated paper honeycomb disks inserted into the exit of the lung box (Figure 2-3).

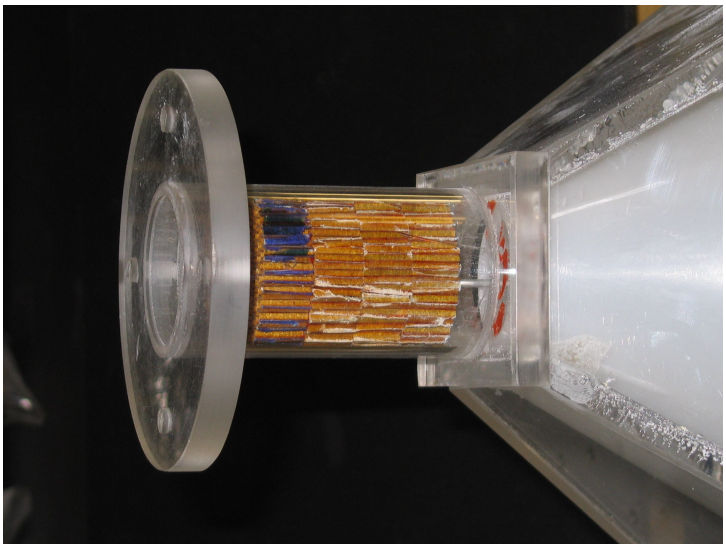

Figure 2-3: Resin coated honeycomb flow straightener in the end of the Plexiglas box

Four 1.27 cm thick pieces were used to achieve a total length of 5.08 cm. This honeycomb would also provide support for the aluminum seed tube to reduce fluctuations in the seed stream. Both the aluminum and the resin coated paper honeycomb had 0.3175 cm hexagonal cells.

As testing was being performed over the course of this research, leaks had developed in the lung box. These leaks were allowing, at times, an estimated 90 percent of the bulk flow to exit the box before entering the test section. Modifications were made to seal the leaks; however, the integrity of the box could not be trusted. A new design needed to be implemented.

2.1.2. Polyvinyl Chloride Lung Tube

Since the transient flow breathing mechanism was not being used for the experiments, the use for such a large reservoir was no longer necessary. A "lung tube" with a simpler design was constructed (Figure 2-4). This was a 3.8 cm diameter PVC pipe with proper seals throughout. One end was left open for the attachment of the inlet structures and test sections.

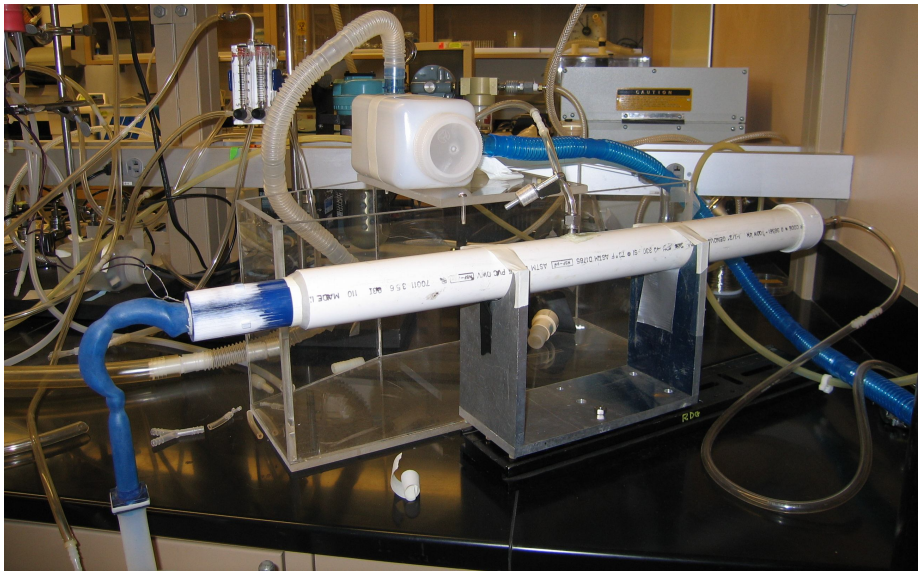

Figure 2-4: PVC "lung tube" for constant flow rate experiments

The bulk flow with a known flow rate enters the lung tube at the rear. The seed flow enters the tube halfway along the length of the tube; the flow rate is also known. A stainless steel 0.635 cm tube extends into the PVC and bends to align parallel with the flow. The stainless tubing continues for 15.24 centimeters. The 0.635 centimeter tubing is then reduced to 0.3175 centimeter aluminum tubing in order to reduce flow

interruptions. The aluminum tubing continues until it is flush with the exit of the PVC. Honeycomb flow straightener was inserted into the end of the tube. This flow straightener acts as a stabilizer for the aluminum seed tube and reduces vortices created in the upstream portions of the tube. There is no mechanism incorporated into this apparatus that would allow a transient flow to be generated.

2.2. Breathing Mechanism

Whereas, the experiments of this research endeavor were conducted using a steady flow rate, this is not realistic for actual human respiration. A device was needed in order to displace air in the lung box and create an inspiratory breathing pattern. Any work done to develop this breathing mechanism was completed before the use of the simplified lung replica was implemented. The transient flow was not used for experiments reported herein.

2.2.1. Speakers

The original idea for a breathing mechanism was two loudspeakers. Kicker Comp VR dual voice coils were used. Using a Stanford Research Systems Function Generator (Model DS 335) and a McIntosh Audio Amplifier (Model MC 50) the maximum displacement of the speakers was measured. It was determined that the speakers would not provide sufficient displacement to generate the required breathing pattern. The accuracy of the speaker operation is also not sufficient. Another method needed to be used to displace the air in the lung box.

2.2.2. Piston-Cylinder Device

In order to achieve more displacement a piston-cylinder device was constructed out of PVC pipe, Teflon (PTFE) disks, and linear actuators. The cylinders are made out of 15.24 centimeter schedule 80 PVC with a 20.32 centimeter flange to attach to the lung box. Teflon disks with a 15.24 centimeter diameter and thickness of 5.08 centimeters were used as the piston faces. Teflon helps to minimize friction at the walls while still achieving a tight fit. Two Smart Motor model 1720 linear actuators were purchased from Ultramotion. The actuators are mounted to the back of the cylinder using aluminum mounts. Figure 2-5 shows a detailed drawing of the linear actuator. Figure 2-6 shows the lung box assembly with the piston-cylinder devices attached.

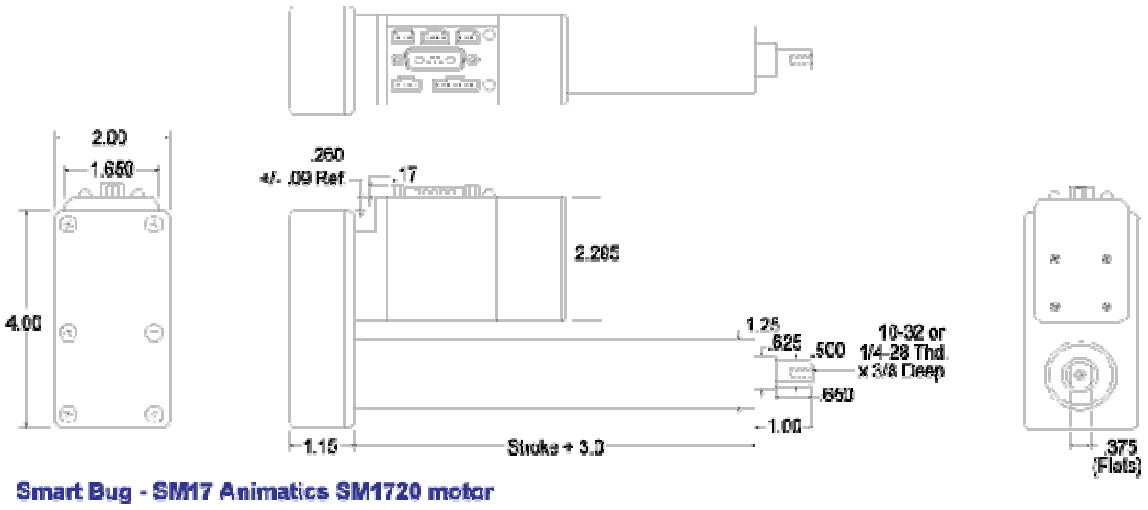

Figure 2-5: SmartMotor linear actuator

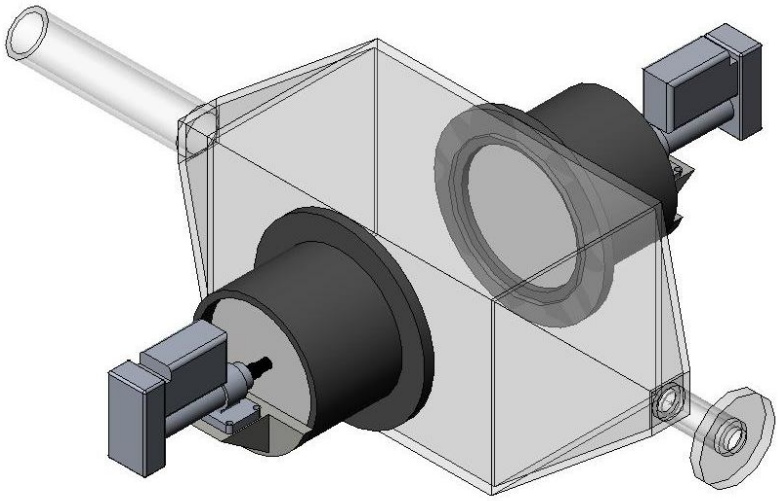

Figure 2-6: Lung box with piston-cylinder devices

2.3. Breathing Pattern

A constant flow rate was used throughout the entirety of the research discussed in this thesis. This simplification allowed experimental methods to be tested without the additional complication of a transient flow. The reality of a transient flow was considered and steps were taken to implement a breathing pattern, however no actual data collection was conducted using this flow.

2.3.1. Constant Flow Rate

The original flow rate is based on the peak flow rate that occurs during light activity breathing, assumed to be 680 milliliters per second or 40.8 liters per minute. Due to the specific aim of this research, controlled aerosol delivery, the flow could not be uniformly seeded. Therefore, a separate flow needed to be established for the seed

particles. In order to obtain flow results not affected by a shear layer, the bulk flow and seed flow rates are adjusted so that the flows were nearly velocity matched at entrance to the test models. In the course of the research, glass tubes with inlet diameters of two centimeters were used in testing, alternately, with two different oral airway models, both with 2.16 cm diameter inlets. The following table (Table 2-1) shows the velocity matched flow rates for both 2 and 2.16 cm diameters. Two different seed tubes were used for testing. When the glass tubes were used, an aluminum seed tube with a 0.159 centimeter inside diameter was used and when the oral airways were used, a seed tube of one millimeter inside diameter was used.

Table 2-1: Velocity matched flow rates

Co-Flow (slpm)	Seed Flow Velocity Matched with Oral Airway Models (sccm)	Seed flow Velocity Matched with Glass Tubes (sccm)
1.00	2.15	6.30
2.00	4.29	12.60
3.00	6.44	18.90
4.00	8.58	25.20
5.00	10.73	31.50
6.00	12.87	37.80
7.00	15.02	44.10
8.00	17.16	50.39
12.00	25.74	75.59
20.00	42.91	125.99
41.00	87.96	258.27

The area change in the oral airway model caused an increase in velocity and therefore pushed the flow into the turbulent regime. The flow rates needed to be reduced in order to maintain laminar flow throughout the entire trachea model. Calculations were

performed in order to find the maximum Reynolds number throughout all the test models. The calculations determined that a flow rate of 27 SLPM would keep the Reynolds number at 2000 through the tubes with a 2 cm diameter. As for the oral airway, the region yielding the highest Reynolds number was the glottis region. The diameter of the glottis of the glass model is estimated to be 0.95 cm. The resin model was designed with a 0.83 cm diameter in this region. A flow rate of 12 SLPM co-flow was calculated to be the maximum flow rate in order for the flow to remain stay out of the fully turbulent regime. A bulk flow rate of 8 SLPM or less is needed in order for the flow to remain laminar throughout. Through experimentation, however, the highest flow rate that led to a non-uniform seed stream at the exit of the oral airway model was 2 SLPM. This is an order of magnitude lower than the light activity breathing, which may be a difficult breathing rate to maintain. Despite this possible difficulty, testing was continued using the low flow rate of 2 SLPM. There is much experimental uncertainty with all of the flow rates used for this research except the later experiments performed with a 2 SLPM flow rate. This flow rate is measured with accurate devices.

2.3.1.1 Flow Meters

For the testing done at the Applied Energy Research Lab (AERL), Teledyne Hastings Mass Flow Meters metered the flows. These flow meters were calibrated to work in the ranges needed. A HFM-200H flow meter calibrated in the 0-1 SLPM range was used to meter the seed flow. A HFM-201 calibrated for the 0-100 SLPM range was used for the bulk flow. The flow meters were checked some time into the research and deviated far from the calibration. It is unsure how much of the preliminary results with

the hollow glass spheres and the diesel smoke have the correct flow rates. The flow meters were sent to the company for recalibration before the final testing with the incense was performed.

2.3.2. Transient Flow Rate

An actual human respiratory pattern takes a sinusoidal shape (Figure 2-7).

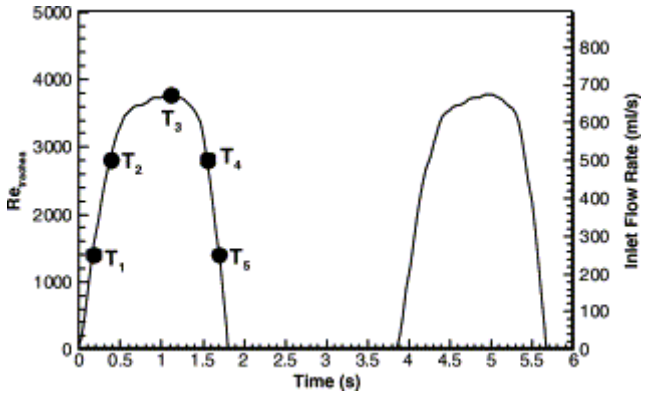

Figure 2-7: Light activity inhalation pattern

The sinusoidal waveform, however, is not the ideal form for targeted drug aerosol inhalation. The ultimate goal would be to manipulate the human breathing pattern into a square waveform. Obviously, a square waveform is not a feasible breathing pattern for a human inhalation. A true square waveform is also impossible to generate with the linear actuators; there needs to be some acceleration time. Using the Smart Motor Actuation software supplied with the purchase of the linear actuators, a program was written to

control the linear actuators. Paul Mobley did a majority of the work programming the linear actuators. Figure 2-8 is a read out of the linear actuator path.

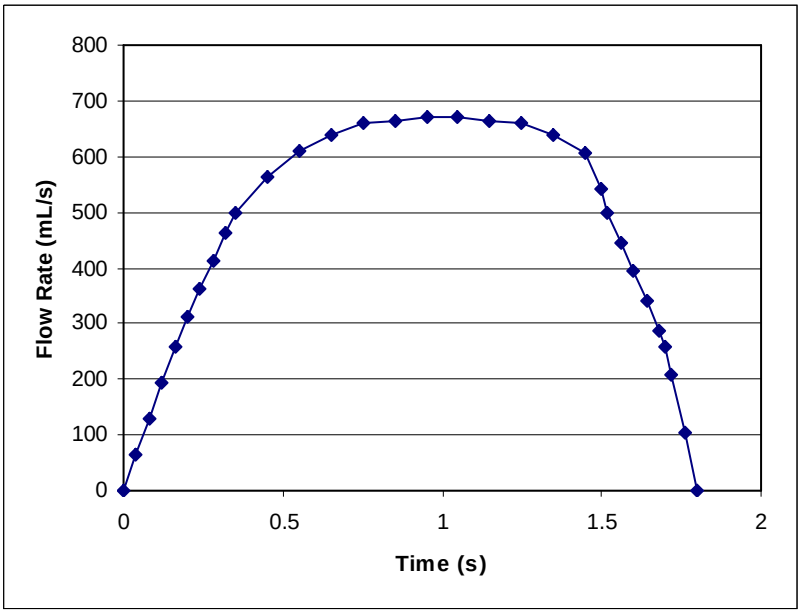

Figure 2-8: Breathing pattern created by linear actuators

Further information regarding the programming of the linear actuator in order to create a breathing pattern is in Appendix A – SmartMotor Linear Actuator Data.

2.4. Airway Models

In order to study the different segments of the flow, a series of models were constructed with increasingly complex geometry. Basic straight, constant area tubes were used as a first stage. Constant area tubes with a 90 degree bend were then used as an intermediate step between the straight tubes and the oral airways. Two different oral

airways were constructed using different methods. Bifurcating bronchial airways were also constructed to attach to each of the respective oral airways.

2.4.1. Glass Transition Tube

The exit of the lung box has a diameter of 3.81 centimeters. The airway models, however, have significantly smaller diameters. A glass piece was made for the transition between the lung box and the airway models.

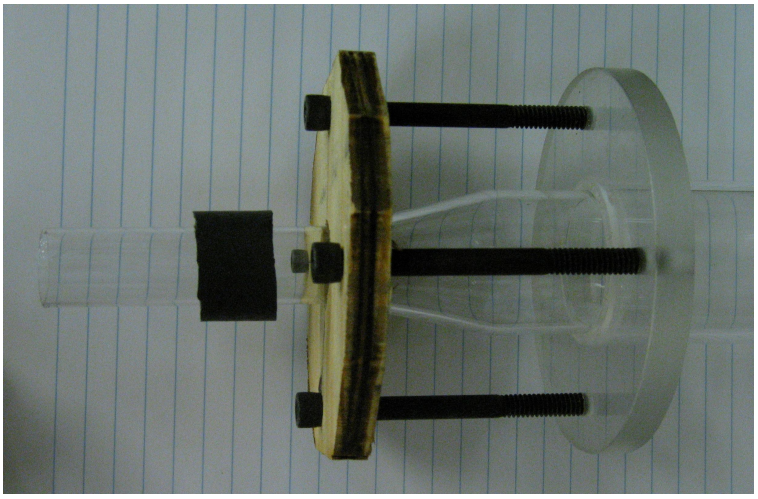

Figure 2-9: Glass transition tube and attachment apparatus

Figure 2-9 shows the transition tube and the wooden brace used to hold the piece onto the lung box flange. A piece of radiator hosing was used to attach the airway models to the smaller end of the transition tube.

2.4.2. Straight Glass Tubes

A series of straight glass tubes were purchased in lengths of 5, 10, 20, and 40 centimeters. The dimensions used were based on the geometry of the oral airway model used in later research. The inside diameter was 2 cm, the representative diameter of the mouth. The rough distance of the flow path through the oral airway is 40 centimeters hence, the use of a 40 centimeter straight tube. The shorter tubes were chosen so that they were one half, one quarter, and one eighth of the longest tube.

2.4.3. Ninety Degree Bend Tubes

The geometry of a human oral airway can be represented, in simplest form, by a glass tube with a 90 degree bend. Two tubes with 90 degree bends were made for the research (Figure 2-10). Like the straight tubes, these were also based on the geometry of the oral airway model, with an inside diameter of 2 cm and comparable lengths.

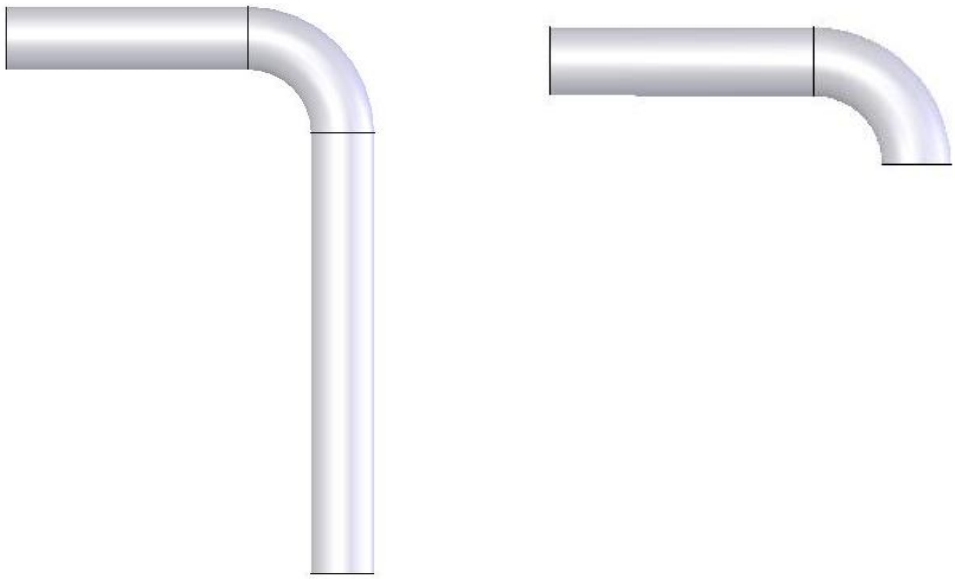

Figure 2-10: Glass tubes with 90^{o} bend: long bend and short bend

The straight entry portion of each bend piece is 7.62 centimeters, and the radius of curvature for the bend is 3.4 cm. The last section of the long bend is 13.97 centimeters; the short bend does not have this final section. These glass pieces were intended to facilitate the study of the flow through a bend, another intermediate step before using the actual oral airway model.

2.4.4. Glass Oral Airway Model

Jan Singhass, the NCSU glassblower, made the first oral airway replica for this research (Figure 2-11). The dimensions used for the model were taken from Cheng et al. (1999). The geometry is based on the cast of an adult male cadaver. Christian McCalley drew the oral airway in Solidworks. He worked with Jan in order get the geometry

correct. No two human oral airways are exactly the same, however, inter-subject variability was not considered in this research.

Figure 2-11: Glass oral airway model made by NCSU glassblower

This model was used for a majority of the Mie scattering data requiring an oral airway. During the testing with this model, it was discovered that the original flow rates (40.8

L/min) were causing the flow to reach the turbulent regime around the voice box (the tightest constriction in the model).

When it became evident that the results using this model were not agreeing with the computational results, planning began for a new oral airway. The method in which the oral airway was made left room for significant human error. The glassblower used a two-dimensional drawing of the model with correct dimensions in order to blow the glass model. Since it was not possible to make measurements of the inside of the model, a new model with a geometry that is closer to the computational model needed to be constructed.

2.4.5. Resin Oral Airway Model

. FineLine Prototyping, of Raleigh, NC, built this precise airway model using a three-dimensional printing method (Figure 2-12). The InVision® HR machine prints thin layers of a thermal resin material, which is cured using ultra-violet light. Once all layers are printed the desired part is finished. Due to confinements on the InVision® machine, the overall length of the oral airway needed to be adjusted. Notice the difference in trachea length on the glass model and the resin model. The portion of the trachea that was left off the oral airway was added to the three generation bifurcating model.

Figure 2-12: Resin oral airway made by FineLine

The process of designing and making this resin model leaves little room for error. The dimensions were taken from the geometry used for the computational testing. One possible drawback of the resin model includes surface roughness which the glass models do not suffer from. The files were modified to include attachment pieces and converted into a form accepted by the Invision® HR machine. The SolidWorks® drawing is shown

in Figure 2-13. The model is made by the machine to the exact specifications of the file. This allowed more confidence in the dimensions and symmetry of the oral airway model.

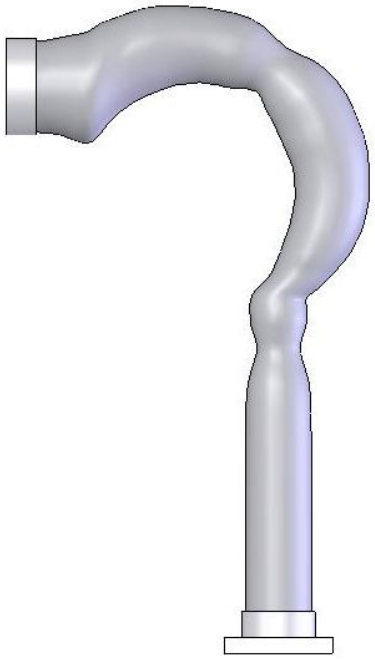

Figure 2-13: SolidWorks model of the resin oral airway model

A collar was drawn on the mouth of the oral airway to allow a tight fit to the flow delivery nozzles. A square flange (Figure 2-14) was designed into the exit of the trachea.

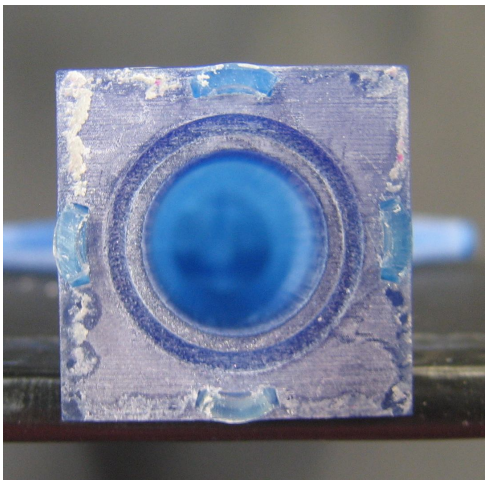

Figure 2-14: Resin flange

The design of this flange is common throughout the set of resin models. When running experiments with just the oral airway the filter holder is attached to the flange. When running tests with the oral airway and the third generation bifurcation, the flanges on each fit together. A 16 mm O-ring fits into the groove to create an airtight seal.

2.4.6. Glass Bifurcations

The scope of this research was intended to include experiments with several generations of bifurcations of the lung. For earlier stages, symmetrically bifurcating airway models were used. The first set of bifurcations was made by Prism Research Glass, of Raleigh, NC. They were made as a modular set so that experiments could be done using just the first generation bifurcation or both first and second generations (Figure 2-15).

Figure 2-15: First and second generation bifurcations built by Prism Research Glass

Although the models were based on the dimensions shown in Table 2-2, these bifurcations were not made with a strong emphasis on dimensions. They do not have smooth transitions between the branches or the correct branch diameters. They served as a simple model for basic flow experiments, until a more accurate model was made.

Table 2-2: Table of dimensions for symmetric bifurcations

	Symmetric				
First		Second		Third	
D1	1.52	D2	1.07	D3	0.75
D2	1.07	D3	0.75	D4	0.52
L1	1.00	L2	1.71	L3	0.19
L2	1.71	L3	0.19	L4	0.24
Rb1	5.02	Rb2	3.50	Rb3	2.46
rc1	0.11	rc2	0.07	rc3	0.05
omega	30^{o}				

The dimensions in Table 2-2 are diameters (D), lengths (L), and radii of curvature (Rb and rc) for the first three generations of symmetric bifurcations in centimeters; they refer to the Figure 2-16.

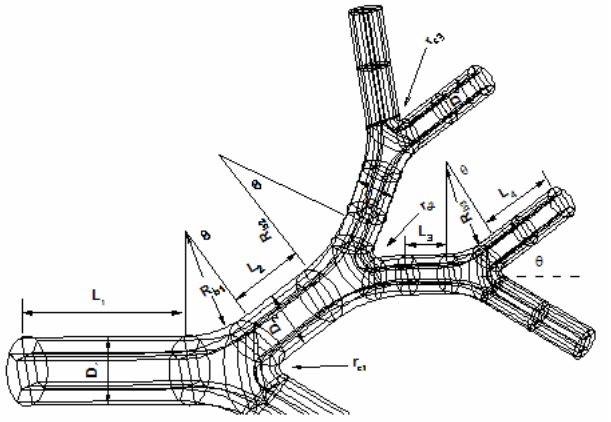

Figure 2-16: Wireframe drawing of G0 – G3 bifurcations

A set of bifurcating airway models needed to be made with more accurate dimensions. For this task, Joe Walas, the glassblower at East Carolina University, was contacted. The new set of models was made with attention to fine and accurate measurements. Models

with two generations of bifurcations (Figure 2-17) and three generations of bifurcations (Figure 2-18) were made.

Figure 2-17: Two generation glass bifurcation blown by the ECU glassblower

Figure 2-18: Three generation glass bifurcation blown by the ECU glassblower

Limited data was collected using these glass bifurcating airway models.

2.4.7. Asymmetric Bifurcation

An actual human airway does not have symmetrically bifurcating lung airways, so asymmetric models should be used based on the geometry in the Figure 2-19.

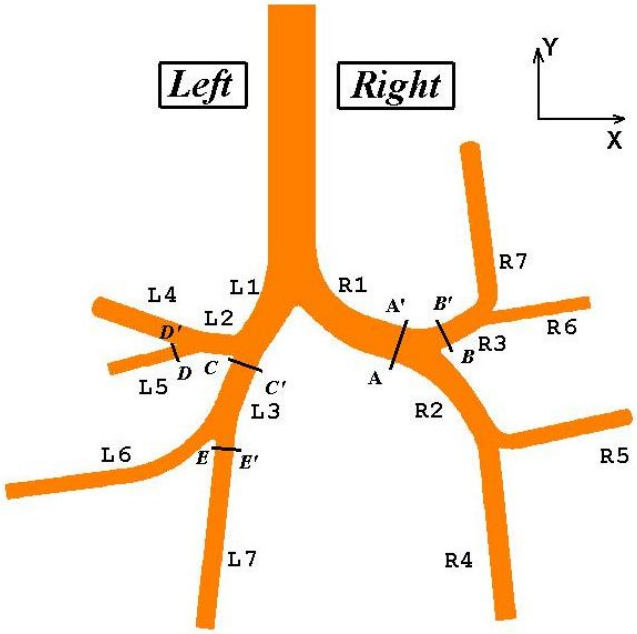

Figure 2-19: Asymmetric bifurcation geometry

The asymmetric first generation glass bifurcating branch made for testing, by Prism Research Glass is shown in Figure 2-20. Limited experiments were run using this model.

Figure 2-20: Asymmetric first generation bifurcation attached to the trachea of the glass oral airway

2.4.8. Resin Bifurcations

Like the oral airway, a set of bifurcations needed to be constructed with dimensions identical to the computational model. The resin method was used to build this new bifurcation model. A part that included first, second, and third generation bifurcations was drawn in Solidworks. This part was drawn to the exact specification of the computational model. The dimensions and wireframe drawing can be seen in Table 2-2 and Figure 2-16. The completed model (Figure 2-21) had a flange that would enable attachment to the resin oral airway model.

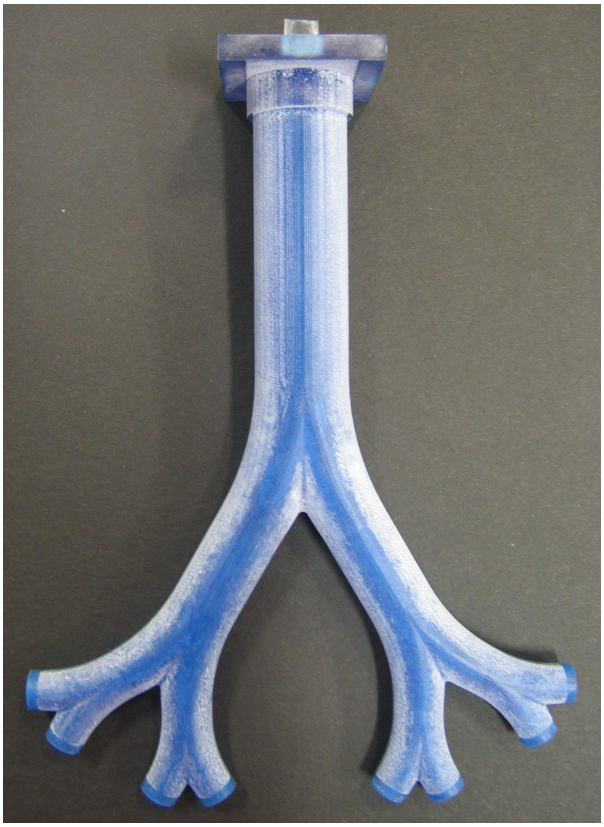

Figure 2-21: Bronchial airway resin model

2.5. Seeding Methods

Finding and successfully applying a material and method to seed the flow proved the most difficult task of this research. Several different materials and methods were attempted and continued investigation is still needed. The ideal particles would be monodisperse with a diameter in the range of 3-10 μm. The ideal method would allow consistent particle delivery at a flow rate on the order of 20 SCCM to meet the velocity matching requirement. The necessity of a low seed flow rate was the most confining

parameter. Most common particle introduction methods use a high velocity spray, which is not a possibility considering the velocity matching requirement.

2.5.1. Hollow Glass Spheres

The first attempt at seeding the flow was the use of hollow glass spheres, specifically, Potter Industries Sphericels® (Table 2-3).

Table 2-3: Hollow glass sphere properties

Sphericel® Typical Properties	
Shape	Spherical
Color	White
Composition	Borosilicate Glass
Density	1.1 g/cc
Particle Size	Mean Diameter 11 microns

These were ideally chosen due to the ability to control particle size and uniformity. The difficulty in using the hollow glass spheres was the seeding apparatus. A fluidized bed atomizer was constructed (Figure 2-22).

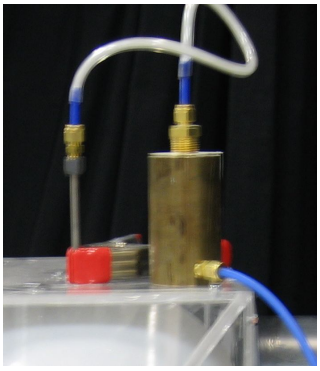

Figure 2-22: Brass atomizer use for seeding the flow with hollow glass spheres

The atomizer has a simple design. A cavity was drilled into a brass cylinder. At the base of the cavity, on a side wall, a 0.159 centimeter hole was drilled offset from the center. The flow enters the cylindrical cavity and creates a swirling effect which fluidizes the bed of particles. The flow, along with fluidized seed particles, then exits through a tube attached to the top. This tube leads to the seed tube of the testing apparatus. This design is a very simple design, which usually yields little to no problems. However, the necessity of a very low flow rate presented problems in seeding consistency. The low flow rate was not sufficient to fluidize the bed of particles, yielding inconsistent results. An apparatus was designed and constructed to split the flow coming from the atomizer. A simple T-shaped fitting was put between the atomizer and the testing apparatus. The use of smaller diameter tubing created flow restrictions in the path leading to the testing apparatus, a majority of the flow was re-routed to exhaust. This allowed a higher flow rate of almost 7 SLPM to fluidized the bed of particles, but the seed flow into the testing apparatus remained at 200 SCCM. Lower seed flow rates could be achieved by

decreasing the tube diameter leading to the testing apparatus or decreasing the initial flow rate. This was successful in yielding better seeding consistency; however, the spheres were still aggregating, an undesirable quality when monodisperse particles are needed.

2.5.2. Diesel Smoke

This experiment requires relatively low flow rates for the flow of seed particles. This constraint presented difficulties in consistency of the seed flow. Although the hollow glass spheres gave decent results, the flow rates were going to have to be reduced and the present seeding system would not be sufficient. A smoke generator derived from a model made at the University of Michigan (Figure 2-23) was constructed.

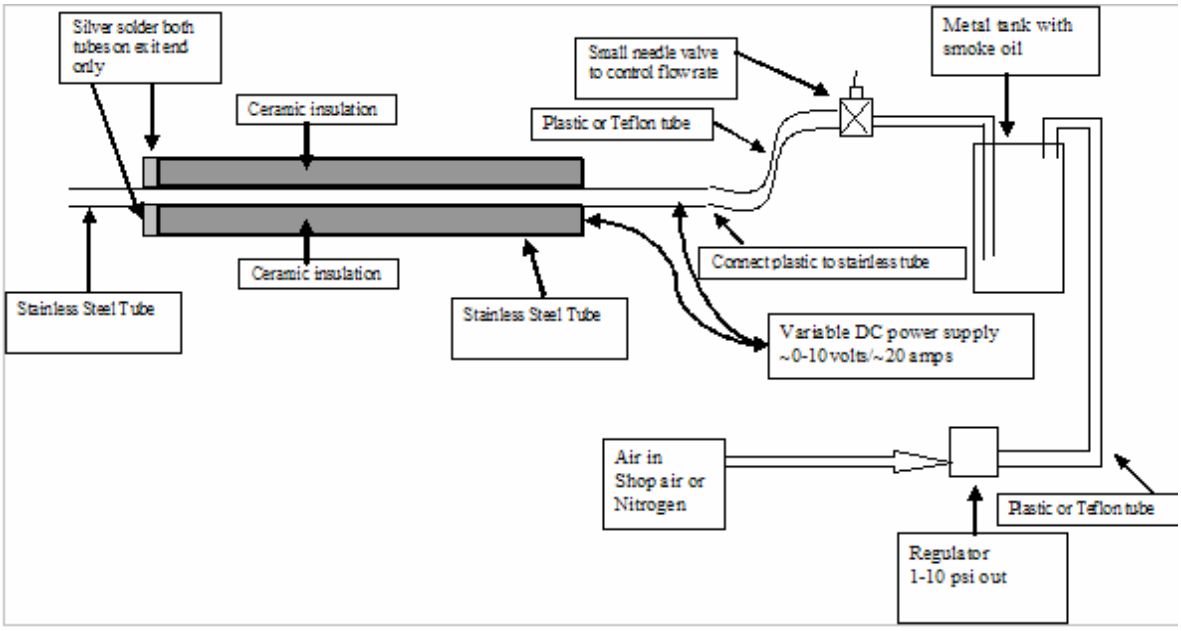

Figure 2-23: Smoke generator (Courtesy of University of Michigan)

The smoke generator used for the current research was a very simplified version (Figure 2-24).

Figure 2-24: Actual diesel smoke generator used for experiments

The main components of the diesel smoke generator are the syringe, the heating tube, the porous plug, and the smoke reservoir. The syringe is filled with diesel fuel and attached to a stainless steel tube. As the diesel fuel is pumped through the tube, the porous plug, fueled by pre-mixed propane-air, heats the tubing. The heated tube causes the fuel to undergo a combination of evaporation and combustion, resulting in what is referred to as smoke. In order to generate a sufficient amount of smoke for the reservoir, the process only requires a few milliliters of fuel. The flow rate of fuel through the tube is important as in too high a fuel flow rate will not allow all the fuel to be converted into smoke. A low fuel flow rate will not yield a high smoke concentration. A disadvantage of using the

diesel smoke apparatus is the safety of the process. Another disadvantage is the ambiguity of the method leads to a lack of documented information about the particle size; particle size is necessary knowledge in this research.

2.5.3. Incense

After deciding the diesel smoke was an unsatisfactory method of seeding the flow, another method needed to be considered. The burning of incense cones was decided upon. The cones were burned in the same reservoir used for the diesel smoke. One cone was able to fill the reservoir with a sufficient quantity of smoke. The seed flow was then sent through the reservoir and then into the testing apparatus. Incense smoke has similar properties to the diesel smoke in that it is polydisperse and contains moisture. The polydisperse characteristic is undesirable, however at this point a monodisperse seeding method was not obtainable using the current flow parameters. Documentation of the size of incense smoke particles varies. The best estimate is that they range from 0.06 to 2.5 μm (Jetter et al. (2001) and Cheng et al. (1995)). Testing was done using incense with the full intent on simultaneously continuing the search for a seeding method that would allow the use of monodisperse particles at a low seed flow rate.

2.5.4. Sodium Chloride and Uranine Dye Aqueous Solution

Dr. Chong S. Kim at the Environmental Protection Agency – Human Studies Division (EPA-HSD), located on the University of North Carolina Chapel Hill Campus, loaned the use of his laboratory, equipment, and supplies for this research. The EPA-HSD has numerous aerosol generators that were not being used at the time. The base

material used in each of these generators was a solution of sodium chloride (NaCl) and uranine dye (fluorescein) in water. The NaCl provided the majority of the particle volume; however, the uranine dye was essential for data acquisition. Each solution contained 0.1 grams of uranine dye; the remainder of the solute was NaCl. The fluorescence of the dye was the needed quality which allowed the location of the particle on the filters to be known. The basic process in each of these generators was the formation of monodisperse droplets which then evaporated leaving particles of known size, based on the concentration of the solution.

2.5.4.1 Condensation Monodisperse Aerosol Generator

The first aerosol generator used was the TSI Model 3470 Condensation Monodisperse Aerosol Generator (CMAG), seen in Figure 2-25.

Figure 2-25: Condensation Monodisperse Aerosol Generator (CMAG)

The process of the CMAG starts with a 20 liter per minute flow of nitrogen with a back pressure of 25 psi through a Collison nebulizer. The terms nebulizer and atomizer are used interchangeably. This nebulizer is said to produce droplets of 3µm diameter. The droplets created by the nebulizer are then evaporated leaving just a particle of, in this case, NaCl and uranine dye. The particles are then sent through a chamber of oil heated to a precise temperature. The oil vapor condenses on the particles creating monodisperse oil droplets. The droplet size is based primarily on the temperature to which the oil is heated. The oil droplets are then reheated and cooled in order to ensure that the droplets are monodisperse. Figure 2-26 shows the schematic of the CMAG.

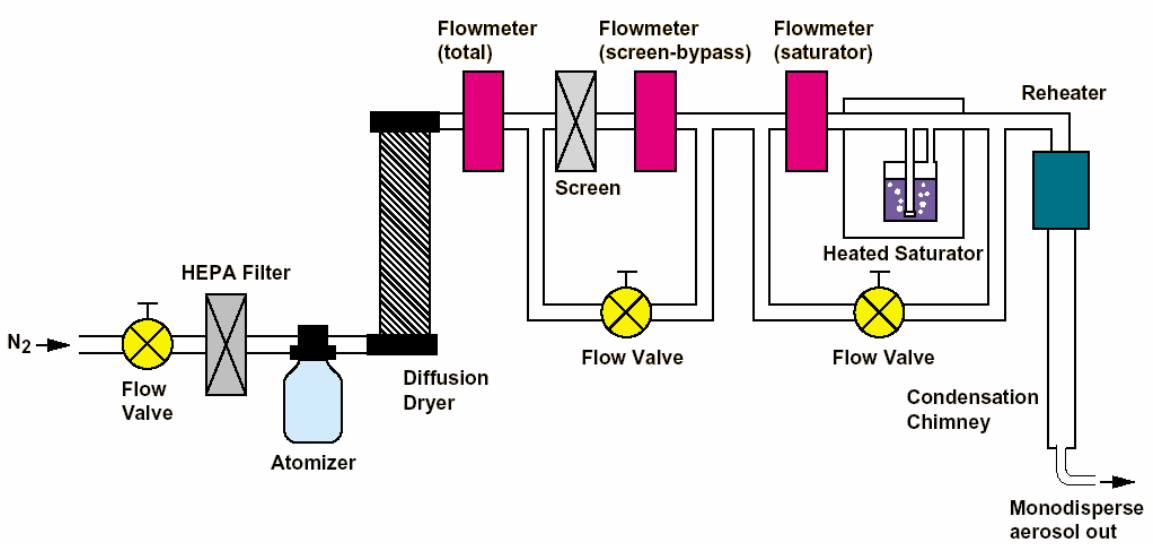

Figure 2-26: Schematic of CMAG

This generator is documented to produce particles in the range of 0.1 to 8 µm, which obviously includes the desired particle size of 3 and 7 µm. Other advantageous qualities of the CMAG are that the particle concentration is high and the nominal flow rate is low.

The generator seemed a good instrument for this research; however, problems arose in the data acquisition. The fluorescent particles being used needed to be activated by water in order to be seen under the ultraviolet light. When the particles were coated with oil the oil shielded the particle from the water needed to activate the fluorescence for the image acquisition process. The method of data acquisition restricted the use of aggressive methods in order to extract the fluorescence.

2.5.4.2 Nebulizer

Since the oil was causing the error, a method of creating particles without the oil was needed. The nebulizer from the CMAG was said to create 3μm droplets with a relatively monodiperse distribution. By creating a solution of the correct concentration, particles of 0.5μm could be created. At that time, the use a solution that would yield larger particle was not guaranteed to work. So as an intermediate step the solution that would yield 0.5μm particles was used. The concern in using submicron particles is the effect of Brownian motion. The closer the particles are to the size of the fluid molecules (in this case air) the more possibility there is of fluid molecules bombarding the particle in an unbalanced fashion leading to random meandering of the solid particles. Brownian motion becomes a concern in this research for particles less than 1μm. After some study of this nebulizer it was determined that a solution that yielded 1 micron particles could be used. Results were obtained using both solutions.

2.5.4.3 Vibrating Orifice Aerosol Generator

The next aerosol generator used was a Vibrating Orifice Aerosol Generator (VOAG), seen in Figure 2-27. The model used for this research was designed and built by Berglund and Liu at the University of Minnesota in 1973. TSI Incorporated carries a newer model of the same generator. Due to limited documentation on the Berglund/Liu generator, the documented information is of the TSI Model 3450. Other than the modern, more compact style of the TSI VOAG there is no difference between the two models.

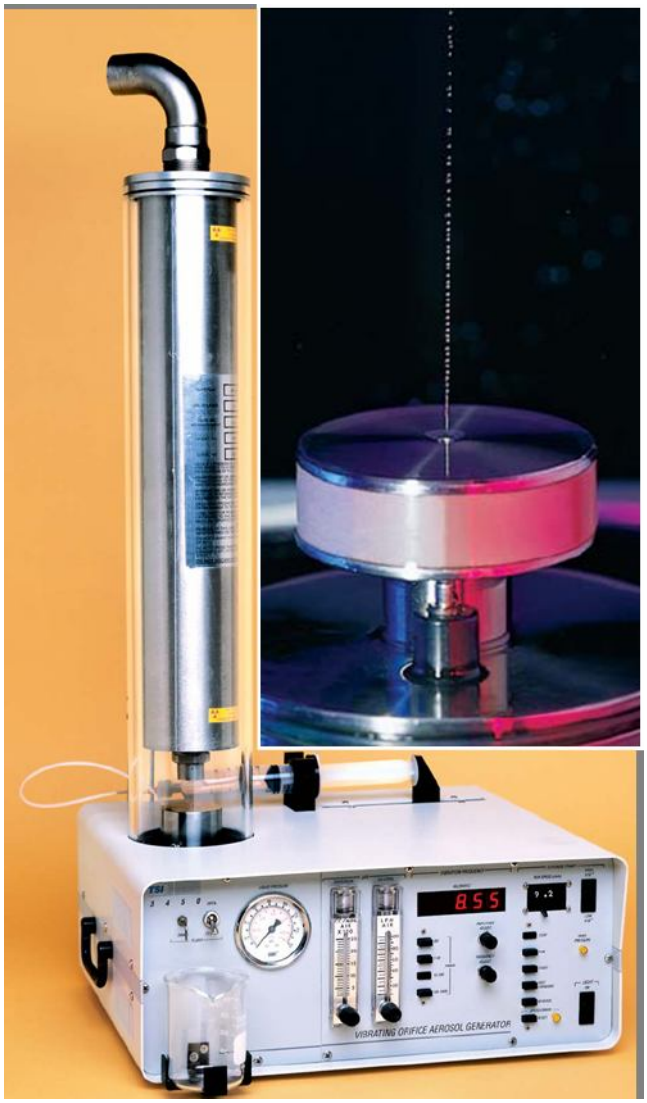

Figure 2-27: Vibrating Orifice Aerosol Generator (TSI Model 3450)

The distinct feature of the VOAG is the piezoelectric ceramic with a small orifice in the center. There are three factors that go into the calculation of desired particle size, D_p: 1) syringe pump rate, Q, 2) vibration frequency, f, 3) concentration of the liquid medium,C.

$$D_p = \left(\frac{6QC}{\pi f}\right)^{1/3}$$

Equation 2-1: Equation used to determine the parameters needed for the desired particle size

If the liquid medium being used does not have a volatile portion, concentration is not a factor. The orifice size is not a controlling factor in particle size, however, it is important to have the correct size orifice for the particle size range to ensure consistency. In this research a 20µm orifice was used. The desired particle size was 7 µm; the three parameters were: a syringe pump rate of 0.139 milliliters per minute, a solution of 0.32% NaCl/uranine dye in water, and a frequency of 45 kilohertz. The solution was pre-filtered in order to remove foreign objects that may clog the orifice; to further reduce the possibility of clogging the solution was also filtered concurrently with operation. The solution was pumped through the orifice. A frequency generator transmitted a signal to the piezoelectric ceramic; this signal created a periodic disturbance in the droplet stream, yielding monodisperse droplets. Dispersion air (15 SCCM) was introduced just after the droplets were produced in order to prevent coagulation of the droplets before entering the drying column. A dilution air of 100 SLPM was then added to the flow in the drying column. Since the VOAG produces a charged aerosol, the drying column also contains a radioactive neutralizer. The flow out of the drying column was then used to seed the flow needed for the research. Figure 2-28 shows the schematic of the VOAG.

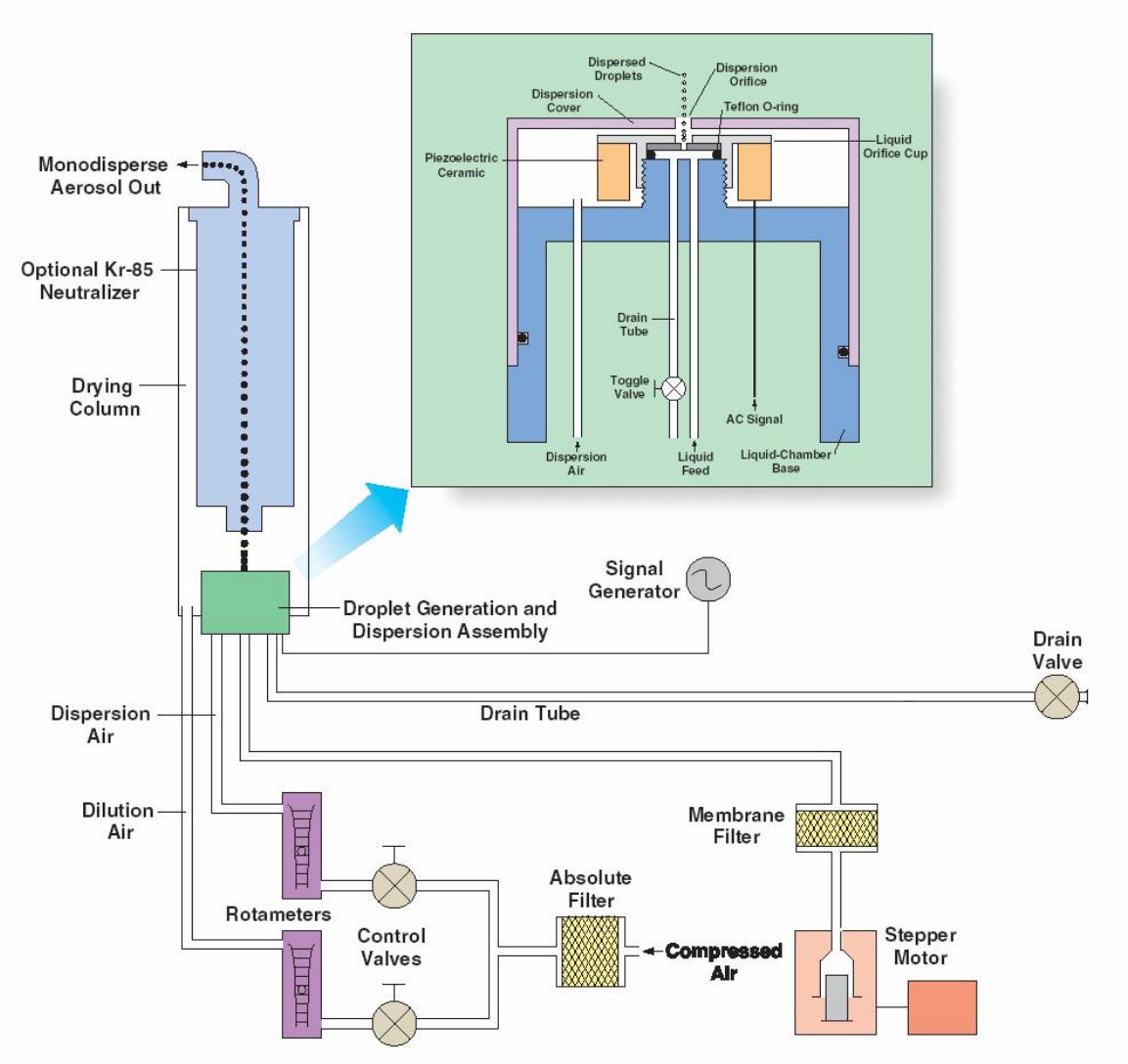

Figure 2-28: Schematic of VOAG

The primary disadvantage of using the VOAG is the low concentration of seed in the flow. The output of the VOAG is a flow of over 100 SLPM and the seed flow rate needed for the research was 20 SCCM. That constitutes a 5000 to 1 ratio of wasted air

and particles to usable air and particles. Run time for each test was very high due to this low concentration.

2.6. Particle Sizing

Knowledge of the particle size is an important aspect of the research, but the means for high fidelity measurements of particle size were not available early on in the research process. Due to lack of access to a particle sizer the experiments were conducted using particles of estimated diameter.

2.6.1. Malvern Spraytec

A new Spraytec aerosol analyzer was made available for use for particle sizing. Spraytec uses a laser diffraction system to analyze the particles. The instrument is intended for high concentration aerosols. After some experimentation it was determined that the Spraytec was not suited for the seed flow used in this research, because the concentrations were not high enough to be detected by the analyzer.

2.6.2. Aerosol Particle Sizer

New software needed to be obtained for the TSI Incorporated Aerosol Particle Sizer Model 3310 (APS 3310) at the EPA-HSD. Once this software was loaded, the APS 3310 was very useful in analyzing the particle flows. Due to the extended period the APS 3310 had been idle a calibration test was performed. Polystyrene latex (PSL) microspheres with known diameters of 1.04 and 2.98 μm were used to check the calibration. The mean diameter of the 1.04 μm microspheres was measured at 1.10 μm

with a geometric standard deviation of 1.08. The 2.98 μm microspheres measured at 2.80 μm with a geometric standard deviation of 1.1. Since the error was within ten percent recalibration was not necessary.

The nebulizer was set up for particle analysis identically to the setup for primary data collection. A 20 SLPM nitrogen (N_2) initial flow entered the nebulizer. An 80 SLPM dilution flow of air was added after the flow exits the nebulizer, so a flow with a total flow rate of 100 SLPM entered the APS 3310. The VOAG was also set up identically to the setup used for primary data collection, with a total flow rate of 100 SLPM.

2.6.2.1 Results of particle sizing

The particles that needed to be analyzed are those produced from the 0.46, 3.7, and 0.32 percent NaCl and uranine dye in water solutions. The 0.46 percent solution was used in the nebulizer to produce particles with an expected diameter of 0.5 μm. One micrometer particles were generated by the nebulizer using the 3.7 percent solution. The 0.32 percent solution was used to generate particles with the VOAG with an expected diameter of 7 μm. The particle sizing results show a significant difference between expected and measured particle size (Figure 2-29).

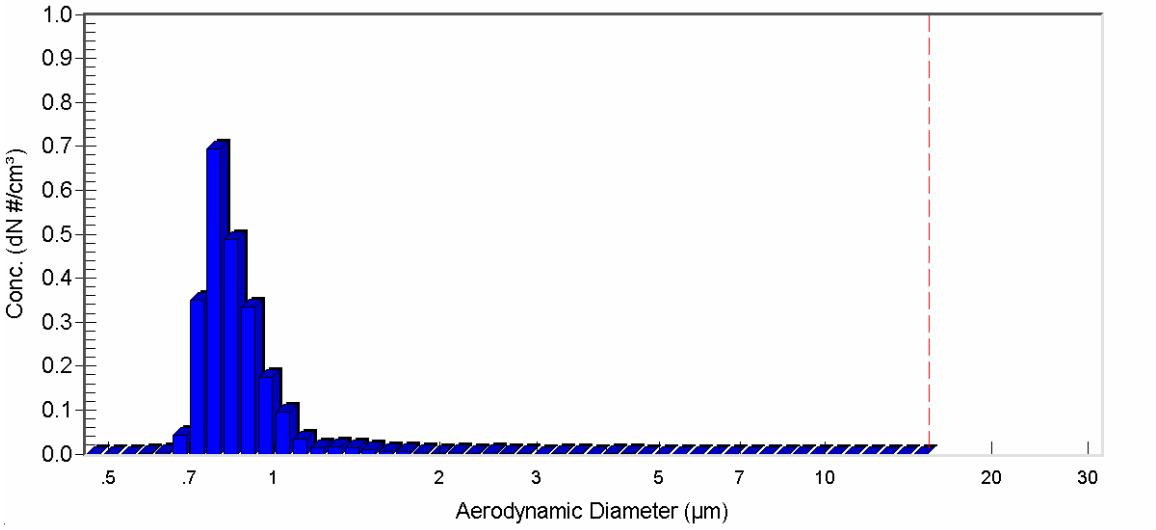

Figure 2-29: Particle sizing results for 0.46% solution

With Collision nebulizers, a common result is having a large range of droplet size. The following table shows the measured data, including, an unexpected low geometric standard deviation.

Table 2-4: Statistical data for 0.46% solution

	Number Particle Size	Surface Particle Size	Mass Particle Size
Median (µm)	0.813	0.851	0.895
Mean (µm)	0.854	0.984	1.23
Geo. Mean (µm)	0.841	0.926	1.07
Mode (µm)	0.777	0.777	0.777
Geo. St. Dev.	1.17	1.35	1.59
Total Conc.	2.30(#/cm³)	5.51(µm²/cm³)	9.03e-04(mg/m³)

The next solution tested was the 3.7 percent NaCl and uranine dye. This solution was expected to produce 1 µm particles through the use of the nebulizer. The following results show a deviation from the expected particle size.

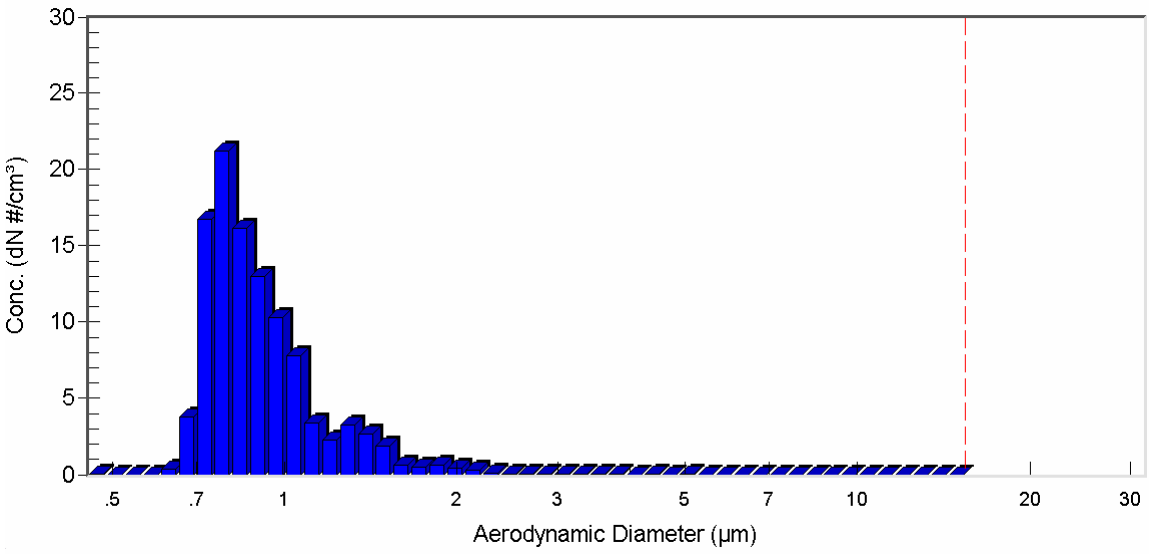

Figure 2-30: Particle sizing results for 3.7% solution

Table 2-5: Statistical data for 3.7% solution

	Number Particle Size	Surface Particle Size	Mass Particle Size
Median (µm)	0.848	0.956	1.07
Mean (µm)	0.924	1.10	1.26
Geo. Mean (µm)	0.898	1.04	1.17
Mode (µm)	0.777	0.777	0.777
Geo. St. Dev.	1.25	1.37	1.44
Total Conc.	106.8(#/cm³)	308.0(µm²/cm³)	5.65e-02(mg/m³)

The last solution used for data collection was used in the VOAG. The VOAG produces much larger initial droplets, therefore, a lower concentration should have yielded a larger

particle size. After measuring the particles, it was obvious that the VOAG was not producing the expected size droplets.

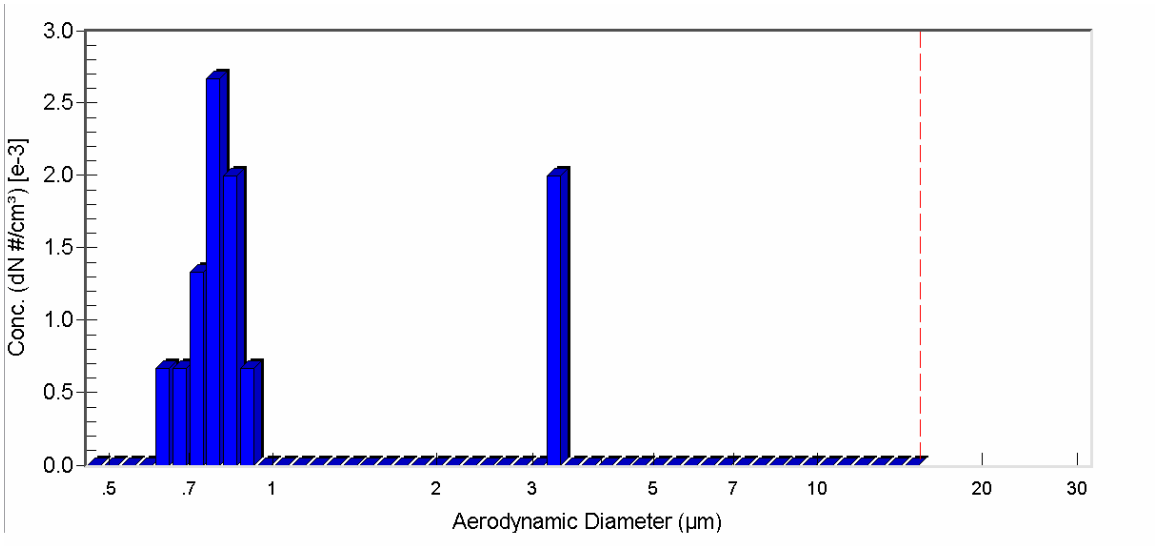

Figure 2-31: Particle sizing results for 0.32% solution

From the figure above, it is evident that there is a bimodal size distribution. The statistical results were, therefore, split into two cases, one for each mode.

Table 2-6: Statistical data for 0.32% solution: Peak 1

	Number Particle Size	Surface Particle Size	Mass Particle Size
Median (µm)	0.778	0.790	0.796
Mean (µm)	0.772	0.785	0.791
Geo. Mean (µm)	0.768	0.782	0.788
Mode (µm)	0.777	0.777	0.777
Geo. St. Dev.	1.10	1.10	1.09
Total Conc.	8.00e-03(#/cm³)	1.51e-02(µm²/cm³)	1.98e-06(mg/m³)

Table 2-7: Statistical data for 0.32% solution: Peak 2

	Number Particle Size	Surface Particle Size	Mass Particle Size
Median (µm)	3.28	3.28	3.28
Mean (µm)	3.28	3.28	3.28
Geo. Mean (µm)	3.28	3.28	3.28
Mode (µm)	3.28	3.28	3.28
Geo. St. Dev.	1.00	1.00	1.00
Total Conc.	2.00e-03(#/cm³)	6.75e-02(µm²/cm³)	3.69e-05(mg/m³)

Steps were taken to investigate why the VOAG was not producing the correct size particles. The syringe pump rate and solution concentration were correct. Many times the frequency generator can be causing the errors; however, after testing the output with an oscilloscope, it was determined that was not causing the error. The orifice was viewed under a microscope to check for corrosion and non-uniformity. The orifice was undamaged. The only other possibilities for error are the connection between the piezoelectric ceramic and the frequency generator or the piezoelectric ceramic itself. Further investigation into the problem with the VOAG still needs to be performed. In summary, the table below shows the calculated particle size, solution concentration, and measured particle size for the three solutions.

Table 2-8: Aqueous solution particle size

Calculated Particle Size (µm)	Solution Concentration (% mass)	Measured Particle Size (µm)
0.5	0.46	0.85
1	3.7	0.92
7	0.32	0.8

2.7. Data Acquisition Methods

Two main methods were used for data acquisition. The method of light scattering referred to as Mie scattering was used for experiments run at the AERL. This method could not be employed for experiments at the EPA-HSD. For these experiments membrane filters were used to filter out particles at the exit of the test sections.

2.7.1. Mie Scattering

The particles employed throughout this research are assumed to be larger than the 488 nm wavelength of the laser emission, therefore the process of light scattering used for image acquisition is Mie scattering. This method was used in testing with the first three seeding mediums: hollow glass spheres, diesel smoke, and incense. A Spectra-Physics 2017 Argon Ion laser, operating at 488 nm wavelength, produces approximately one watt of power.

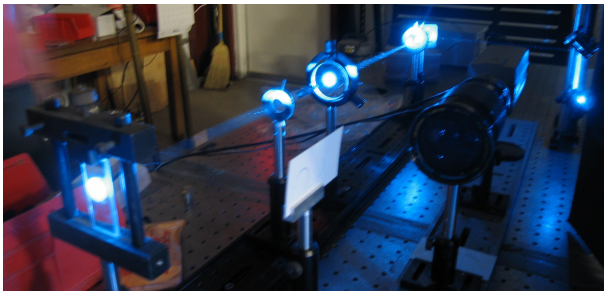

Figure 2-32: Laser beam path

The beam was first reflected through three mirrors in order to orient it correctly. The reflected beam was then sent through a convex lens to expand the beam (Figure 2-32).

The diverging beam was then sent through another lens that collimated the beam. This constant diameter beam was finally sent through a planar lens which converts it into a sheet. This sheet is the desired form for data acquisition. For data acquisition of flow through just the straight tubes the laser sheet needs no more redirection, for the bend pieces and the oral airways the sheet is redirected by another mirror (Figure 2-33).

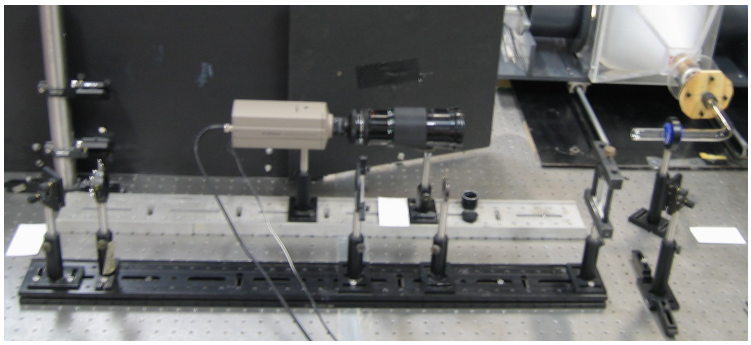

Figure 2-33: Laser optics configuration for 90^{o} glass bends and oral airway models

For the bifurcation experiments, a tower of mirrors was assembled (Figure 2-34), since the airway model needed to built tilted out of the original plane containing the laser sheet.

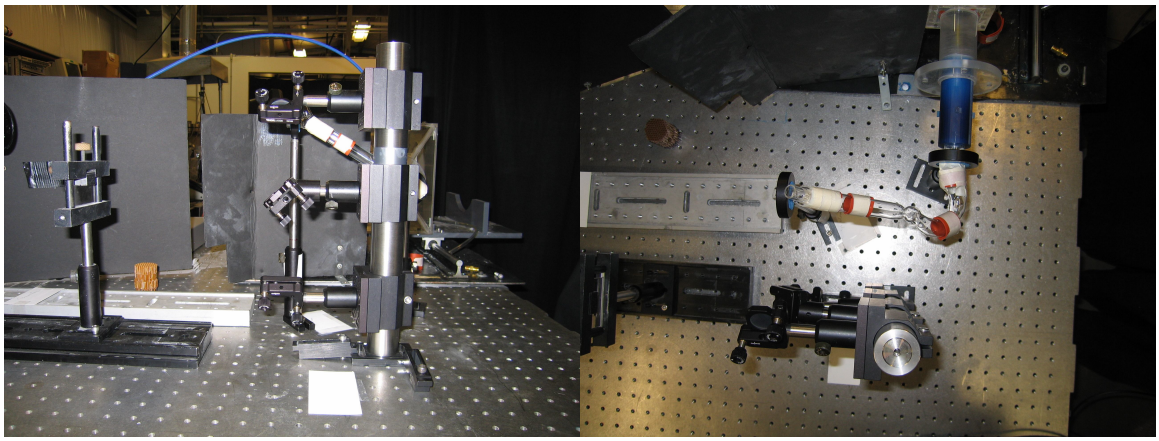

Figure 2-34: Cascade of mirrors used for Mie scattering of flow through the bifurcating models

As the flow exits the airway models, the laser sheet illuminates the seed particles contained in the flow. This illumination enabled the camera to differentiate the particles from the air flow. The particles show up, in the original images, as a light area in the image of the exit cross-section.

A Cohu CCD camera was used to acquire the images. An image acquisition card from Scion Corporation was used to capture individual frames from the video sequence. Scion Image is the software program compatible with this image acquisition card. Still images were able to be captured from the video camera. The still images were converted into binary form, using a thresholding technique for ease of interpretation, as there was little qualitative information in the pixel count. These images were used to determine the spatial location of the particles and not the quantity of the particles.

2.7.2. Membrane Filters

The experiments performed at the EPA-HSD required an alternative data acquisition method. The argon laser being used at the AERL was not able to be transported to the EPA-HSD. The resin models that were made for testing were equipped with filter attachments (Figure 2-35).

Figure 2-35: Filter holder attachment and resin oral airway

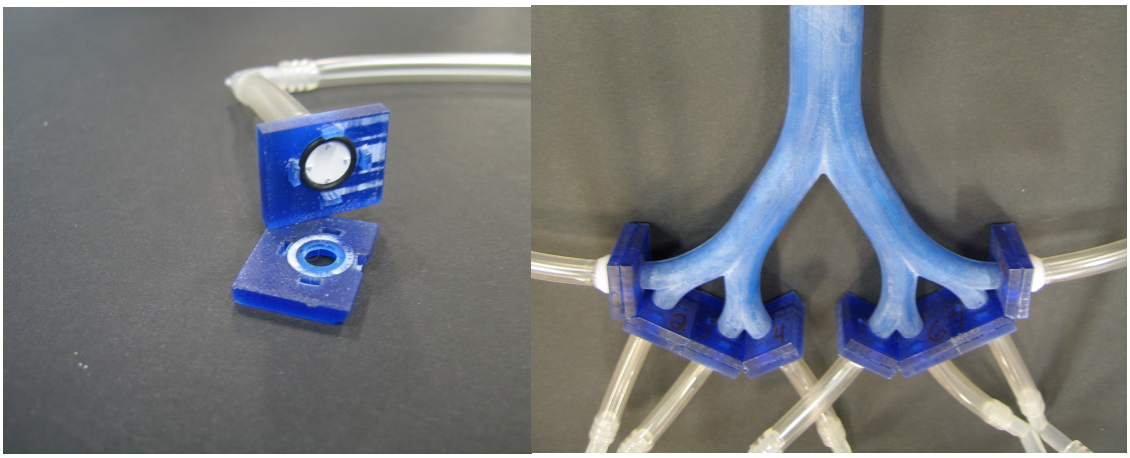

Figure 2-36: Filter holders for three generation bifurcation model a) image of a single filter attachment taken apart b) filter holders attached to the three generation bifurcation model

The filter attachments were designed to hold membrane filters cut with standard size grommet punches (Figure 2-36). Table 2-9 shows the important dimensions for the filter holder apparatus for the oral airway exit, the first generation exit, and the third generation exit. The first generation bifurcation, along with the filter attachments, were not constructed yet, however, all pieces have been designed and the files are ready to be sent off for construction.

Table 2-9: Important dimensions for filter holder attachment

	Oral Airway	First Generation Bifurcation	Third Generation Bifurcation
Exit Diameter	15.2 mm	10.7 mm	5.2 mm
Filter Size (grommet punch)	15.875 mm	11.1125 mm	6.35 mm
O-Ring Inner Diameter	16 mm	11 m	7 mm
O-Ring Width	1.5 mm	1.5 mm	1 mm

Membrane filters were purchased from Millipore. These filters have a pore size of 1.2 μm. The label of pore size is not descriptive of the actual size of the pore; these filters are able to capture particles smaller than 1.2 μm. These filters have been successfully used by Dr. Chong Kim at the EPA-HSD (Kim et al. (1999). The seed particles in the flow are collected by these filters. The filters are removed from the test airways after each test and are stored for safe transport back to the AERL. The argon-ion laser was used to excite the fluorescent dye used in the testing done at the EPA-HSD. The uranine dye has a peak excitation wavelength of 460 nm and a peak emission wavelength of 515 nm. An optics arrangement similar to that of the Mie scattering was used.

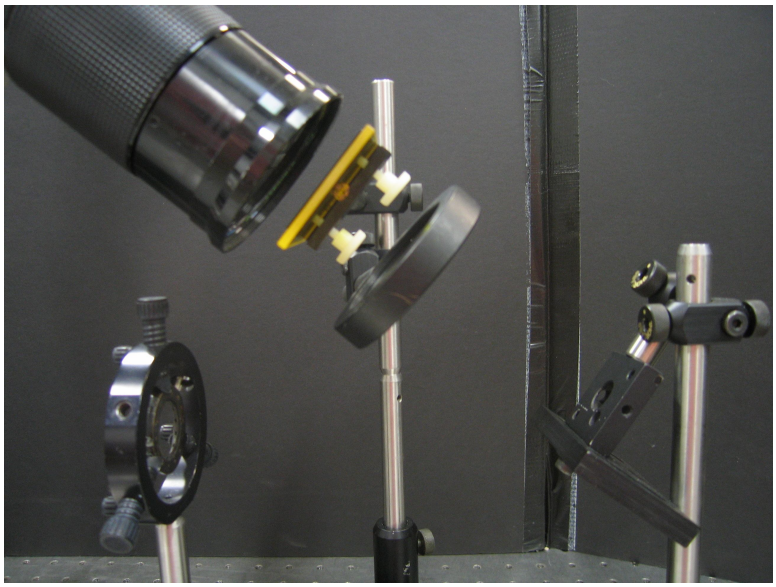

Figure 2-37: Image acquisition setup for use with the membrane filters

Since the desired beam shape was a circular cross-section of slightly less than two centimeters the planar lens was removed. The membrane filter was placed in front of the

beam at a 45^{o} angle so the light on the filter actually created an oval shape. The camera was positioned to accept the light reflecting directly off of the membrane filter (Figure 2-37). Two optical filters were placed between the test filter and the camera lens. The purpose of these filters was to block out unnecessary light to allow for better imaging. The first filter was a 550 nm bandpass filter. Based on the fluorescence properties of the dye this filter should not have allowed the desired wavelength of light to pass (515 nm), however, after trial and error this filter seemed to work the best. The other filter was a sharp cutoff filter. This filter cut off wavelengths less than 500 nm. It was useful in prohibiting reflections of the 488 nm laser light to reach the camera lens. Image acquisition was identical to the Mie scattering method from this point on.

2.8. Stationary Nozzles

The flow delivery was controlled by inlet nozzles. These nozzles allow for the two separate flows to enter the test section in the correct orientation and location. A nozzle with a flexible and controllable seed tube orientation is being designed and constructed concurrently, by Matt Pausley, under the direction of Dr. Stefan Seelecke. The seed tube position will be controlled by shape memory alloy wires. In the meantime, a series of stationary seed tube nozzles have been constructed for testing. The original drawing were made by Joshua Abbe; modifications were made by Matt Pausley. There are five nozzles with similar designs; the difference being that the seed tube exit location has different offsets, measured in percent of the radius. The following images (Figure 2-38) show the five nozzles: 80%, 60%, 40%, 20%, and 0%.

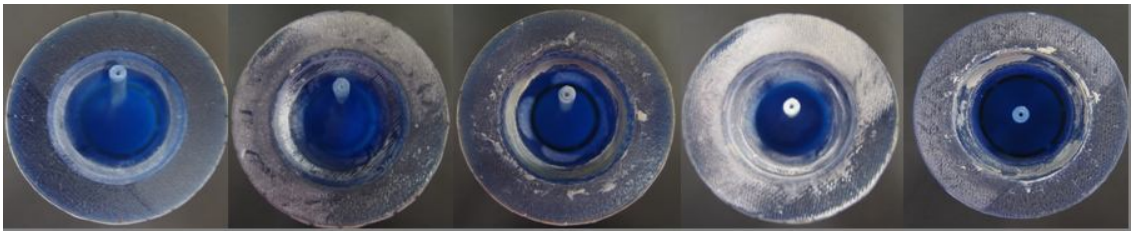

Figure 2-38: Stationary nozzles with radially offset seed nozzle of 80, 60, 40, 30, and 0%

Once these nozzles were introduced into the experiments they acted as the transition from the lung box or lung tube to the test models so the glass transition tube was not necessary.

3.0 Results

Due to the Edisonian nature of this research, there are a myriad of different results to be presented. There are results using different seeding mediums, different apparatus, different flow parameters, and different data acquisition methods. Since there are numerous results of methods and materials used that ultimately did not yield favorable results with useful information, these results are placed in the appendices. The focus of this results section is on the few experiment sets that gave the most complete and accurate results. A table of experiments can be seen in the appendix.

The different data acquisition methods led to some difficulties in comparing images. All results of the 90 degree bend and the oral airways are edited so they could be presented with the same orientation, as shown below in Figure 3-1.

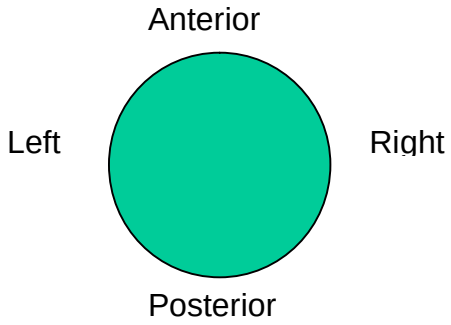

Figure 3-1: Orientation for results images

Values for flow rates are given, but as mentioned before, there is significant experimental uncertainty in these flow rates. These flow rates are what were believed factual at the

time of the test, to find out later they are not correct, with the exception of the results presented with a 2 SLPM bulk flow rate.

3.1. Constant Area Straight Tubes

The first step in airway structures was the constant area straight glass tubes. Since this was the first step in testing a seeding method, the experiments were primarily done to test the basic concepts.

3.1.1. Hollow Glass Spheres

The experiments performed using the hollow glass spheres are not thorough. The original testing parameters were of a light activity breathing rate with a maximum inhalation flow rate of 40.8 standard liters per minute (SLPM). The following results are from experiments run with a bulk flow of 41 SLPM and a seed flow of 23 SCCM. These experiments were conducted using the preliminary airway models. The constant area tubes were attached to the lung box using the transition tube, since the nozzles were yet to be constructed. The seed injection location was in the center of the entrance to the test section. Due to the lack of ability to measure accurately, the exact location is unknown. Comparing the images in Figure 3-2, it can be seen that the seed stream location in the cross-section is very similar for each of the straight glass tubes.

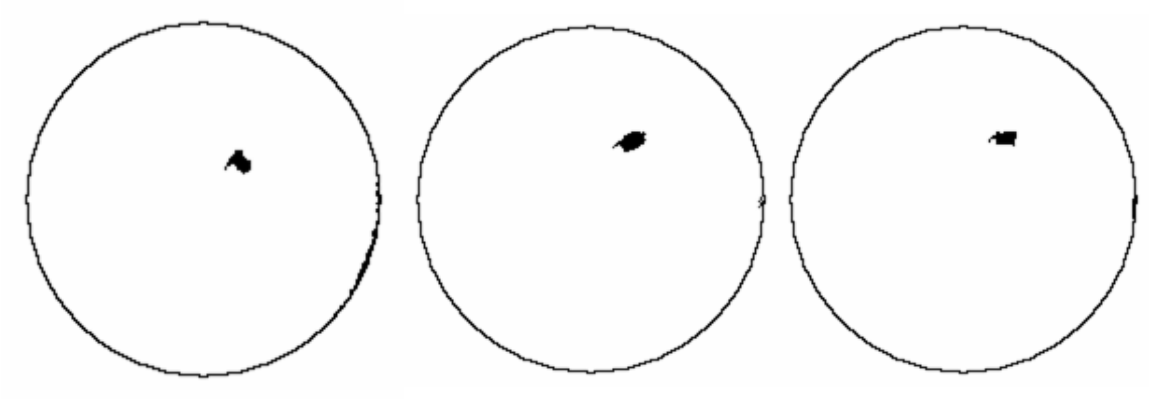

Figure 3-2: 5, 10, and 20 centimeter straight tube results

The slight difference is due to the rudimentary positioning of the seed tube. The seed tube is a simple aluminum tube. Initial seed tube location was the approximate center. The seed tube can not be guaranteed to be parallel with the bulk flow, therefore the longer the test section the more offset the seed stream becomes.

3.1.2. Incense

The comparison of flows using the different nozzles was of interest. An 8 SLPM bulk flow rate with a seed flow rate of 10 SCCM was used for these experiments. Experiments were run using the nozzles with the seed tubes that were offset 40% and 80% of the radius. The seed stream in the images of the flow through the 80% nozzle is much less concentrated than the 40% nozzle. These images can be seen in Figure 7-6.

3.1.3. Velocity Matching Results

With the difficulty of measuring the flow rates, determining how sensitive the two phase flow was to the velocity matching of the bulk and seed flows was important. A simple test using the 20 centimeter straight tube was performed. The resin nozzles with 0, 20, 40, and 60% offset seed tubes were attached to the lung tube. The bulk flow rate was set and maintained at 8 SLPM. The seed flow rate was adjusted from 5 to 50 SCCM in 5 SCCM increments (10 SCCM increments for the 0% case). These results are presented in Figure 7-2 through Figure 7-5. The flow rates in these experiments are the correct values; these tests were run after the recalibration of the flow meters.

It was interesting to find that the flow was scarcely affected by changing the seed flow rate by an order of magnitude. Due to the lack of dependence the flow has on velocity matching, the subsequent experiments were conducted using a seed flow rate of 10 – 20 SCCM without close attention to the velocity matching parameter. Another observation made from these experiments was that the nozzle with the 20% offset seed tube seems to yield results very similar to the nozzle with the 40% offset seed tube. This could be a result of the 20% offset nozzle not being parallel to the flow in the nozzle exit plane. Fortunately, a limited number of experiments were run with the 20% nozzle.

3.2. Constant Area Ninety Degree Bend

The effect a 90 degree bend had on the two phase flow was an important intermediate step before testing the complex geometry of the oral airway.

3.2.1. Hollow Glass Spheres

The 90 degree bend was first used with the hollow glass spheres as the seed medium. Figure 3-3 shows the flow exiting the long 90 degree bend. The seed stream exits the 90 degree bend along the posterior edge.

Figure 3-3: 90 degree bend

This is the expected effect; as the flow underwent the 90 degree bend the particles momentum carried them across streamlines towards the posterior edge of the model.

Once the flow straighteners were added to the apparatus a new set of experiments were run. The following schematic (Figure 3-4) shows the seed injection location for the set of tests run with the flow straighteners.

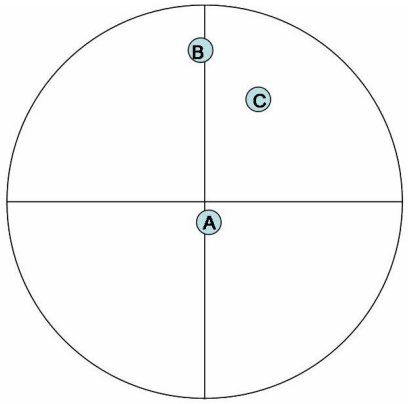

Figure 3-4: Seed injection location for first experiments with flow straighteners

Five cases were run with one of the above seed injection locations (Figure 3-5). All tests were done using a 41 SLPM bulk flow rate. The first three cases have a seed flow of 200 SCCM. The seed flow was adjusted for the fourth test. The seed flow rate could not be measured concurrently with the tests so the exit seed flow rate for test four was not known. This test was done to experiment with the effect of non-velocity-matched flows. The fifth test had the same parameters as the first test.

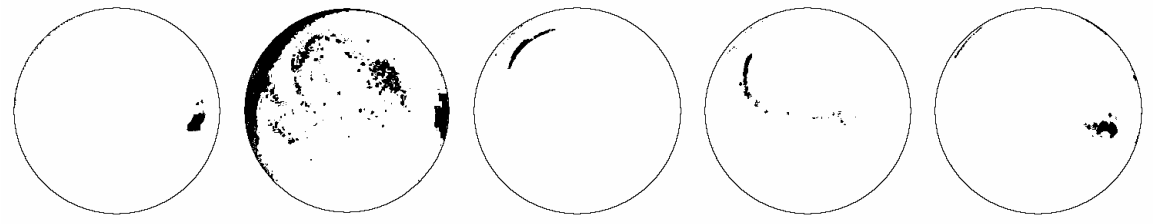

Figure 3-5: Five cases of flow through the long bend

The cases run with the B or C seed injection locations seemed to have a less compact seed stream at the exit of the test section. This is possibly due to the seed injection location being outside the radius of the test section entrance, therefore the seed stream must go through a convergence through the transition tube before entering the test section. The seed stream emitting from the more central seed injection location, may be less affected by the convergence.

3.2.2. Diesel Smoke

For the following tests, the flow rates were reduced to coincide with a Reynolds number of 2000 through the glass 90 degree bend model. The bulk flow was adjusted to 27 SLPM and the velocity matched seed flow rate is now 40 SCCM. There are three seed injection locations tested using the diesel smoke through the 90 degree bend: a central location, a left location, and a far left location. In later tests, the left and far left locations would be referred to as a 180 degree position.

3.2.3. Incense

Limited experiments were run using the 90 degree bend with incense. Some results can be seen in the appendix coupled with the straight tube results for incense. Figure 7-6 compares straight tube results with the 90 degree bend results.

3.3. Glass Oral Airway

Being available early on in the research process, the glass oral airway was used for numerous experiments. This was the first step in a more realistic geometry. The oral airway added a great deal more complexity to the flow path.

3.3.1. Hollow Glass Spheres

The acceptable results from the 90 degree bend, with the central seed injection location, led to the trial of the glass oral airway. One test was run with the glass oral airway model; the seed at the exit of the model was a uniform cloud covering the entire cross-section. The flow was moving into the turbulent regime at some point in the oral airway. This is what led to the need to re-determine the actual Reynolds numbers.

3.3.2. Diesel Smoke

After results of the long bend were studied, the oral airway model was subjected to tests. A number of different flow rates were used before determining that 8 SLPM would be the highest flow rate that could be run through the oral airway. Once 8 SLPM was decided on as the flow rate to be used, experiments were done with the oral airway model injecting the seed flow at the center, left, right, top, and bottom. Like the left position, the others were also given numerical labels later in testing. The top location refers to 90 degrees, bottom: 270^{o}, and right: 0^{o}. Figure 3-6 shows the injection angles for experiments run with the oral airway. A circle is drawn at the 40% of radius location. It is important to note that the injection angle is not referring to the angle in reference to

the flow, it is the angle in relation to the 0^o vertical from the base of the mouth to the roof. The seed tube is oriented parallel to the bulk flow.

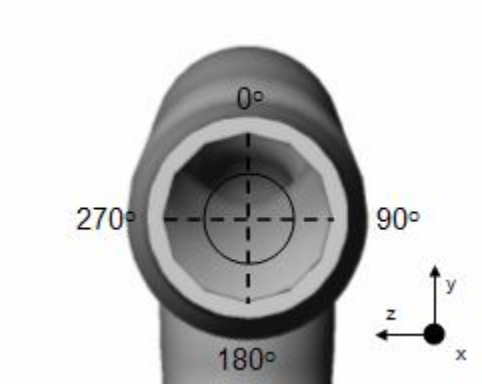

Figure 3-6: Injection angles and 40% radius circle for oral airway experiments, looking into the mouth of the oral airway

The assignment of injection angles to the top, bottom, left, and right designations may seem counter-intuitive (left is 180^o). The reason for this is that for testing done at the AERL, the bend models and oral airways are positioned parallel to the ground where gravity pulls in the direction of the right side of the models. Originally, when straight tubes were being used, the seed injection locations were assigned relative to the Plexiglass box outlet. The conventions in Figure 3-6 are used for the remainder of the experiments.

Note that the aluminum tube was used for seed injection. The exact position of the aluminum tube within the entrance of the test section is not measured. The images taken of the aluminum tube protruding from the honeycomb is the best representation of seed injection location.

3.3.3. Incense

The results with the glass oral airway are the first step towards a realistic flow path. Original experiments were run with the 40% offset nozzle and an 8 SLPM flow rate. The results of four cases using 8 SLPM can be seen in Figure 7-10. Once it was determined there was an error in the flow rates, tests were run with the 2 SLPM flow rate. Also using the nozzle with the 40% offset seed tube, cases were run for 24 seed injection location in 15 degree increments (Figure 3-7). It was promising that the seed stream was not a uniform cloud at the exit.

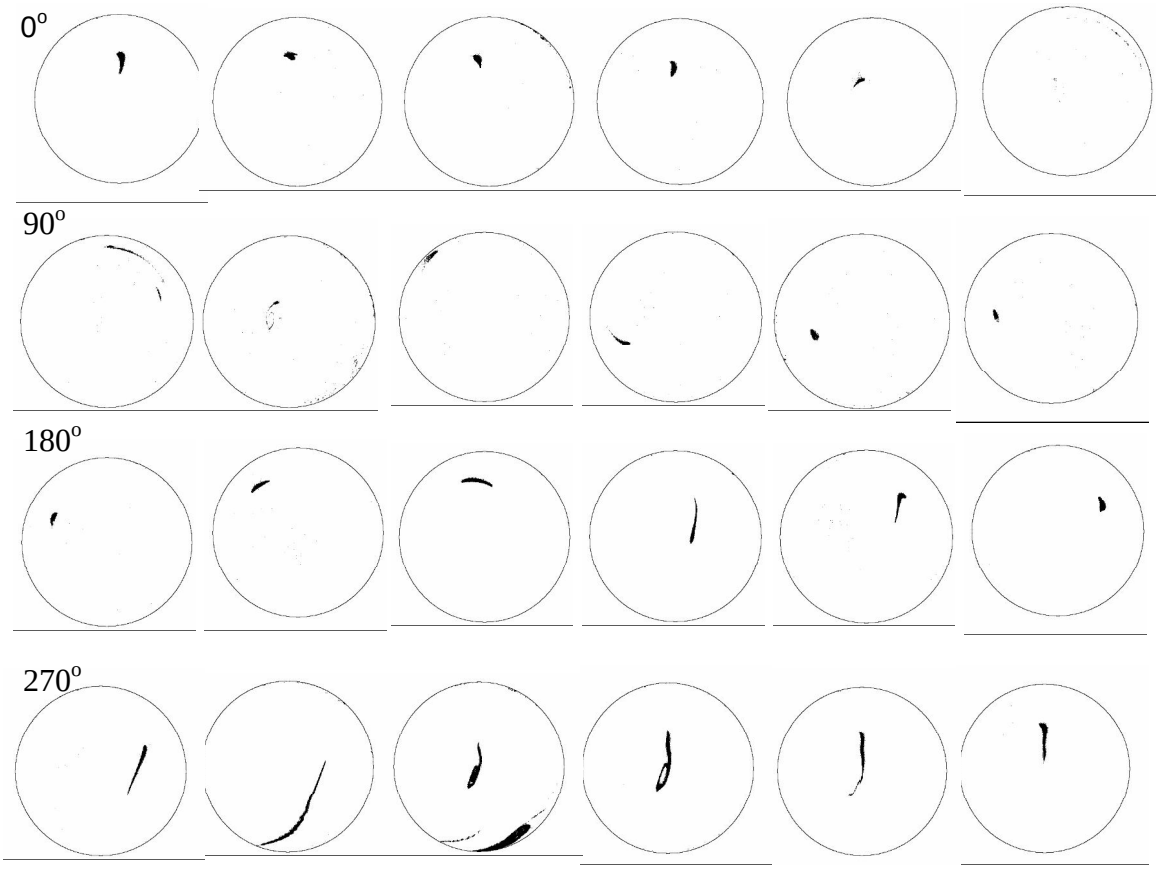

Figure 3-7: Results from glass oral airway using a 2 SLPM flow rate, starting in the top left corner is the 0° case, increasing 15 degrees each image from left to right

From 0° to 270° (with the exception of 75° through 105°) there is a compact seed stream that steps its way around the cross-section.

3.4. Glass Bifurcations

A number of different models of glass bifurcations were attached to the oral airway to add complexity. The first set of bifurcations was a simple symmetric branch. For another set of experiments, a set of second generation branches could be attached to

each of the two first generation branches. The final model of glass bifurcations used for experiments was the simple asymmetric first generation bifurcation. All experiments performed with the glass bifurcations employed the use of incense as the seeding medium.

3.4.1. Symmetric First Generation

Once data was collected using the oral airway it was necessary to test the first generation of the bronchial bifurcation. The glass bifurcation model used was the one built by the ECU glass department. This set of experiments was performed using the nozzle with the 40% offset seed tube. The nozzle was rotated between taking images so that data could be collected for 24 seed injection locations (Figure 3-8). A bulk flow rate of 8 SLPM and a seed flow rate of 10 SCCM were used.

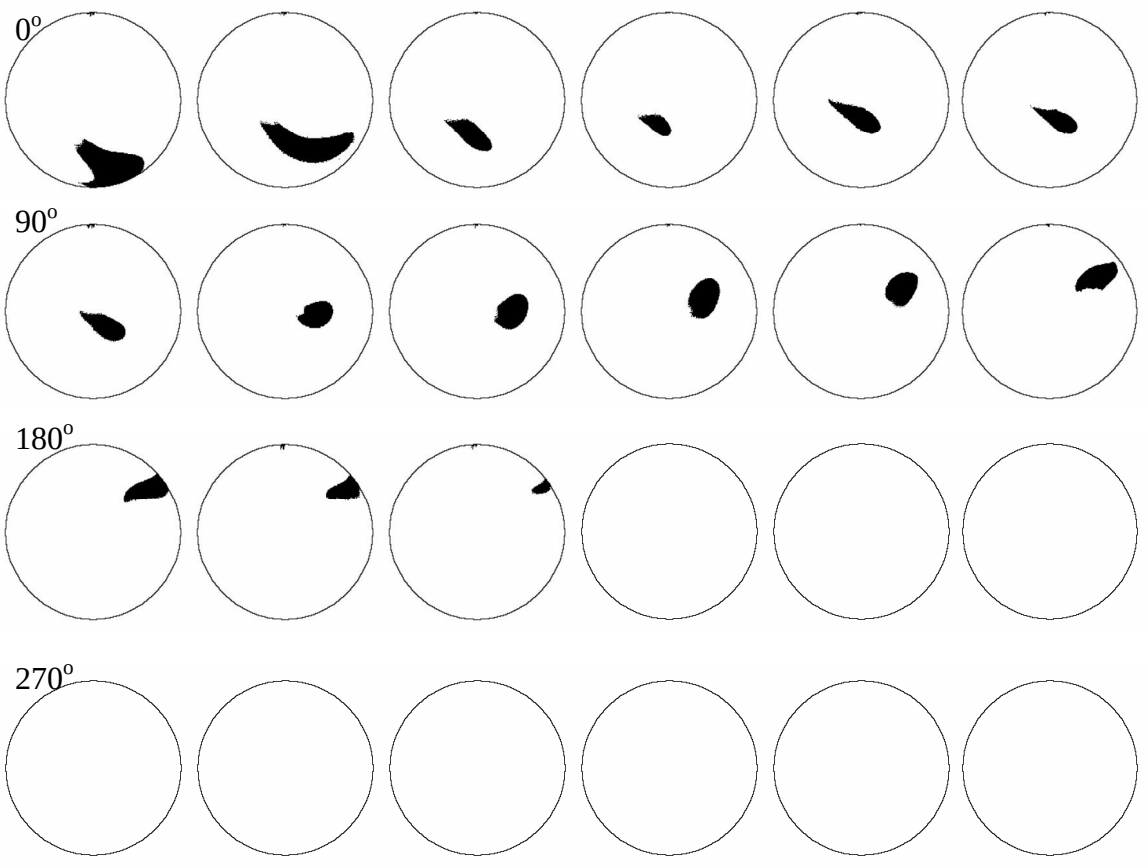

Figure 3-8: First generation right branch (G1.2), full set of 360° in 15° increments from left to right

There is a distinct pattern in the seed stream as the release angle changes. Starting along the posterior edge in the 0° case the seed stream gradually move towards the anterior edge, then at about 75° begins a gradual move towards the right edge. Using the first data acquisition method, flow exiting two different branches could not be investigated concurrently. The following test (Figure 3-9) is a separate set of experiments for the left branch, but with the same parameters as the right branch.

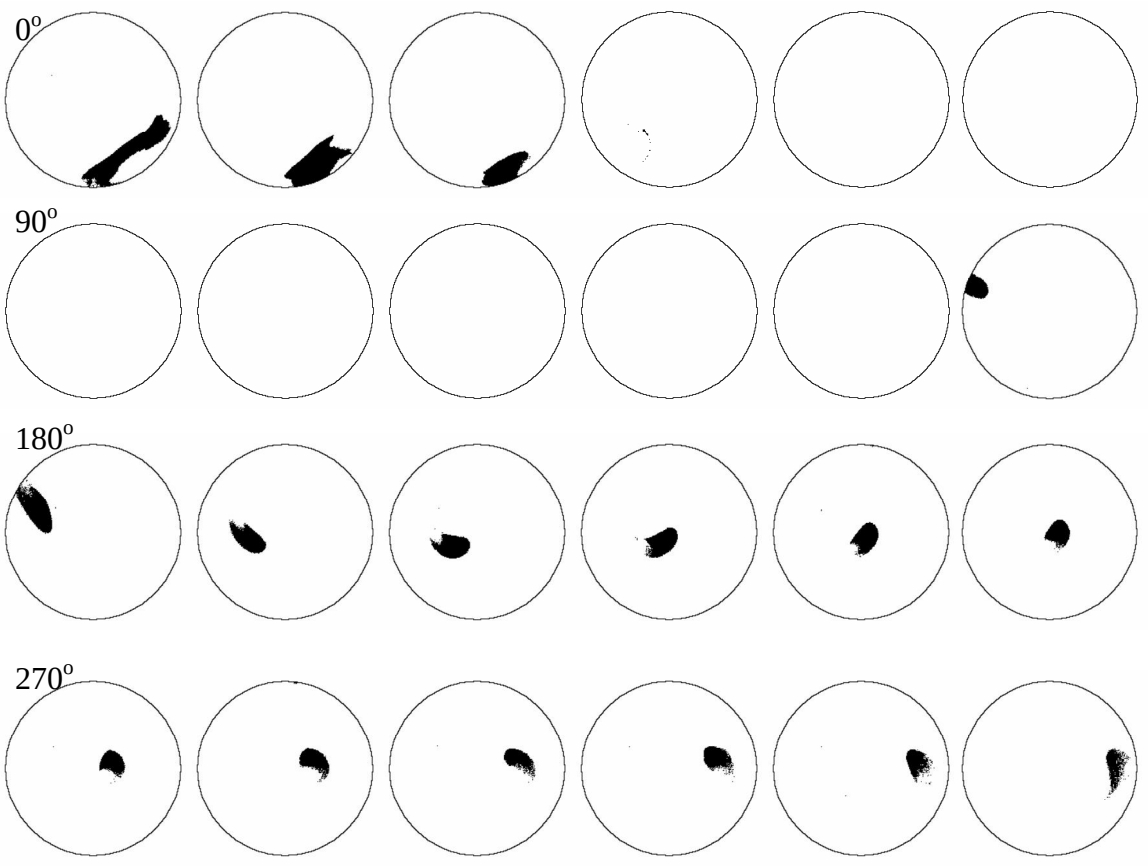

Figure 3-9: First generation left branch (G1.1), full set of 360° in 15° increments from left to right

Part of the seed stream exits both of the branches in seven cases, 0°, 15°, 30°, 165°, 180°, 195°, and 210°. The flow results using the 180° seed injection location show a good representation of the seed stream splitting into the two branches (Figure 3-10).

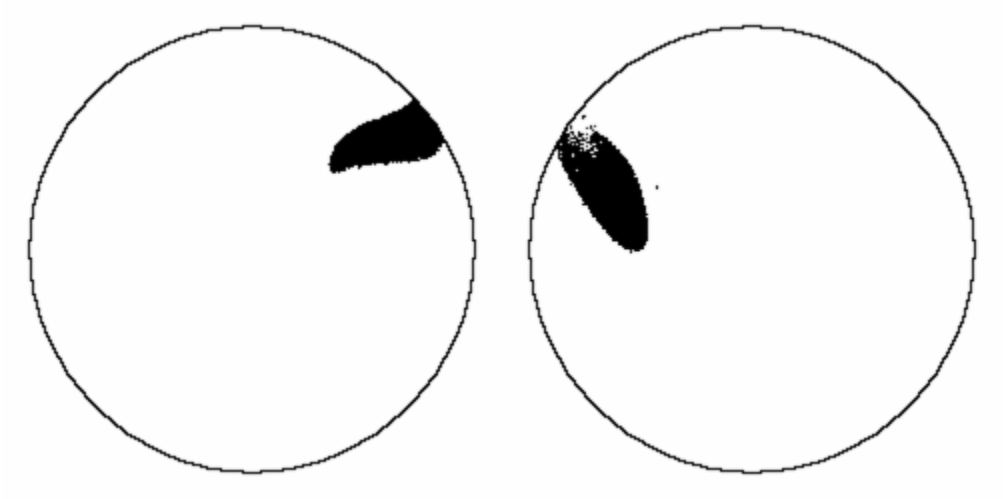

Figure 3-10: 180^{o} seed injection location results in symmetric first bifurcation

3.4.2. Symmetric Second Generation

Only a sampling of second generation data was collected. A full set of 24 cases in 15^{o} increments were run to test the seed stream at the exit of the right most branch (G2.4). These results are presented in the appendix, Figure 7-11. The bulk flow rate was 8 SLPM. The nozzle with the 40% offset seed tube was used to control the particle injection location. Without the results from the other three outlets a full discussion of these results is difficult. It is important to note however that the seed stream is present in only half of the cases (240^{o} through 45^{o}).

3.4.3. Asymmetric First Generation

The symmetric model of the bronchial bifurcations gave useful results of how the flow reacts to branches and decreasing areas; the next stage was to test a more realistic

geometry of a human airway. The first generation asymmetric bifurcation was fitted onto the glass oral airway to test this modification. A flow rate of 8 SLPM was used with a seed flow rate of 10 SCCM.

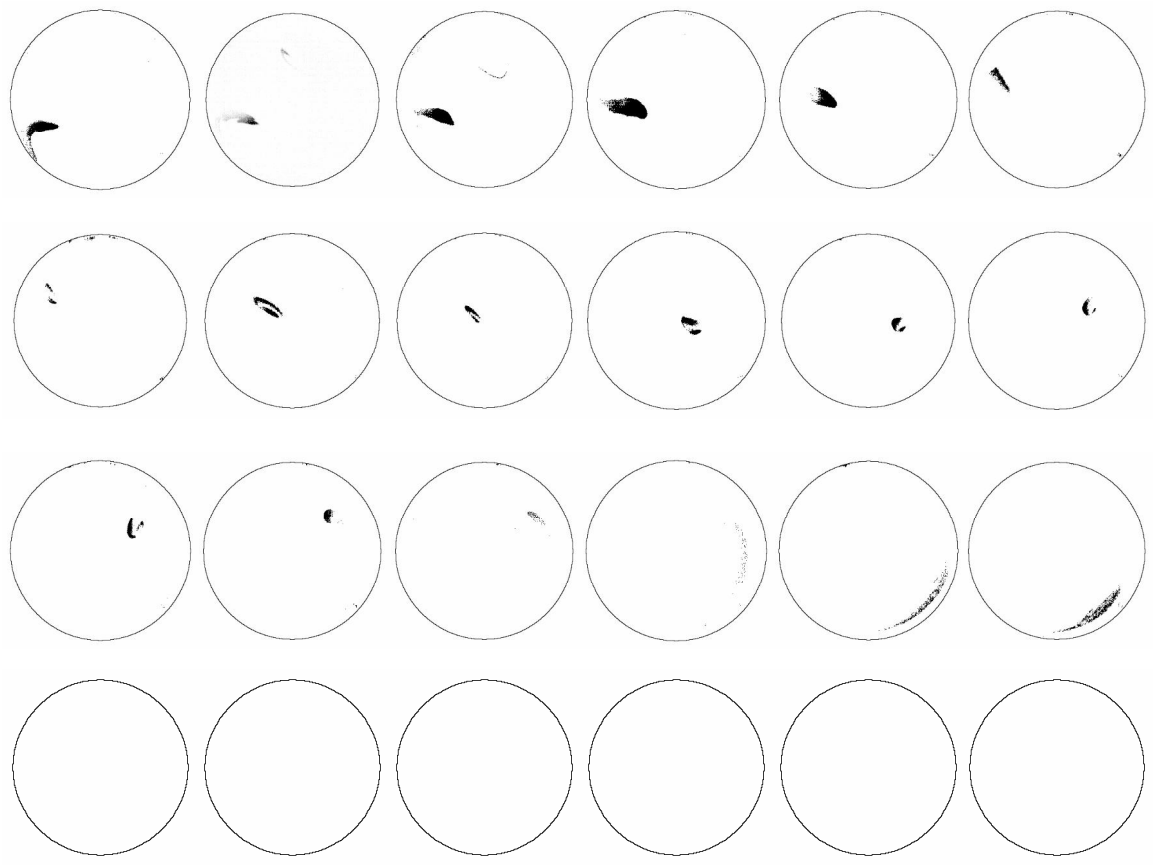

Figure 3-11: Asymmetric first bifurcation left branch (G1.1), full set of 360^{o} in 15^{o} increments from left to right

Once again the data acquisition restricts the obtaining of results of both the left and right branches concurrently. A separate set of experiments were conducted for the right branch (Figure 3-11) with the same parameters as the left branch (Figure 3-12) experiments.

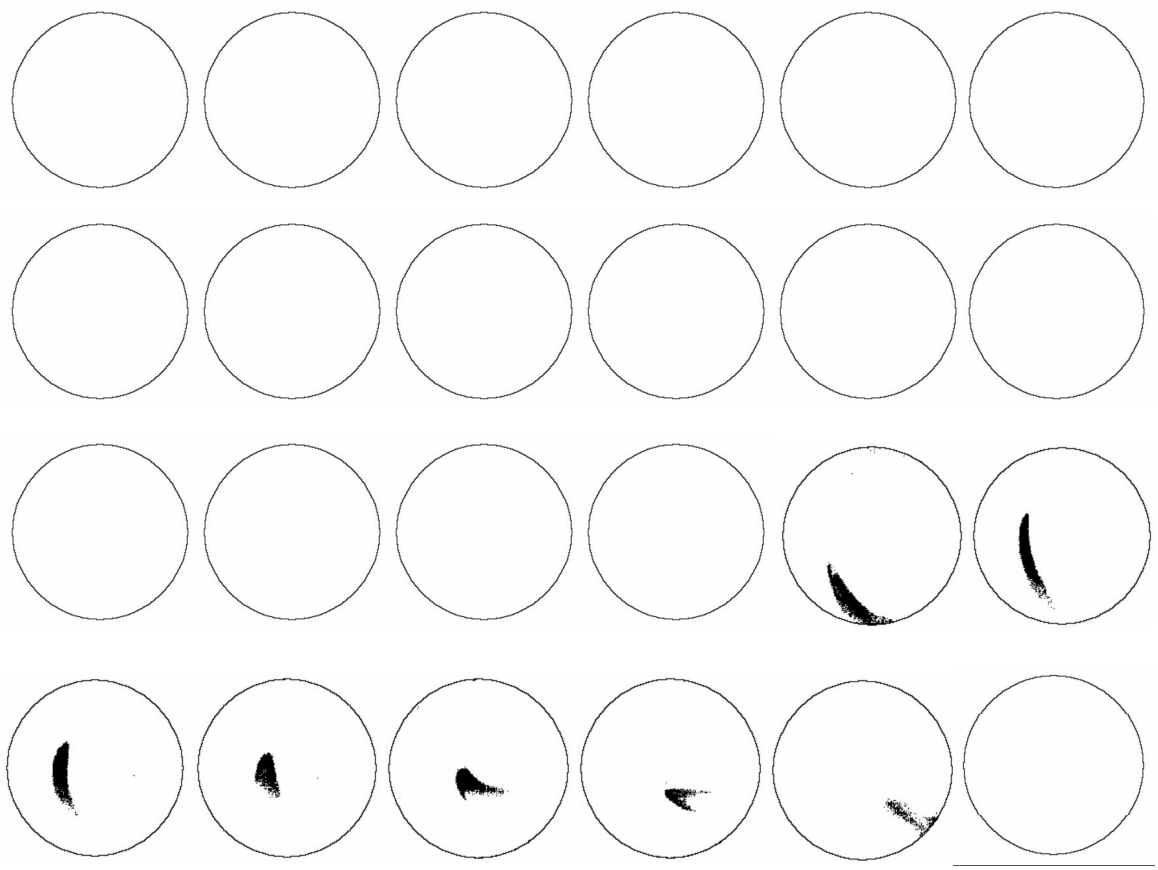

Figure 3-12: Asymmetric first bifurcation right branch (G1.2), full set of 360^o in 15^o increments from left to right

Since the right branch branches off the trachea at a larger angle, it was expected that more of the seed stream would follow the bend with a lesser magnitude. There are only two cases where the seed stream goes through both branches: 240^o and 255^o. The asymmetry of the bifurcations makes predicting the flow behavior more difficult than the symmetric cases.

3.5. Resin Oral Airway and Bifurcation

The results from the resin oral airway were important, because the geometry is now identical to the computational model. The resin oral airway was used for experiments performed with incense and sodium chloride particles from the nebulizer and the VOAG. The three generation resin model was used in experiments performed with sodium chloride particles.

3.5.1. Incense

A full set of results for a 2 SLPM flow rate through the nozzle with the 40% offset seed tube is shown in Figure 3-13.

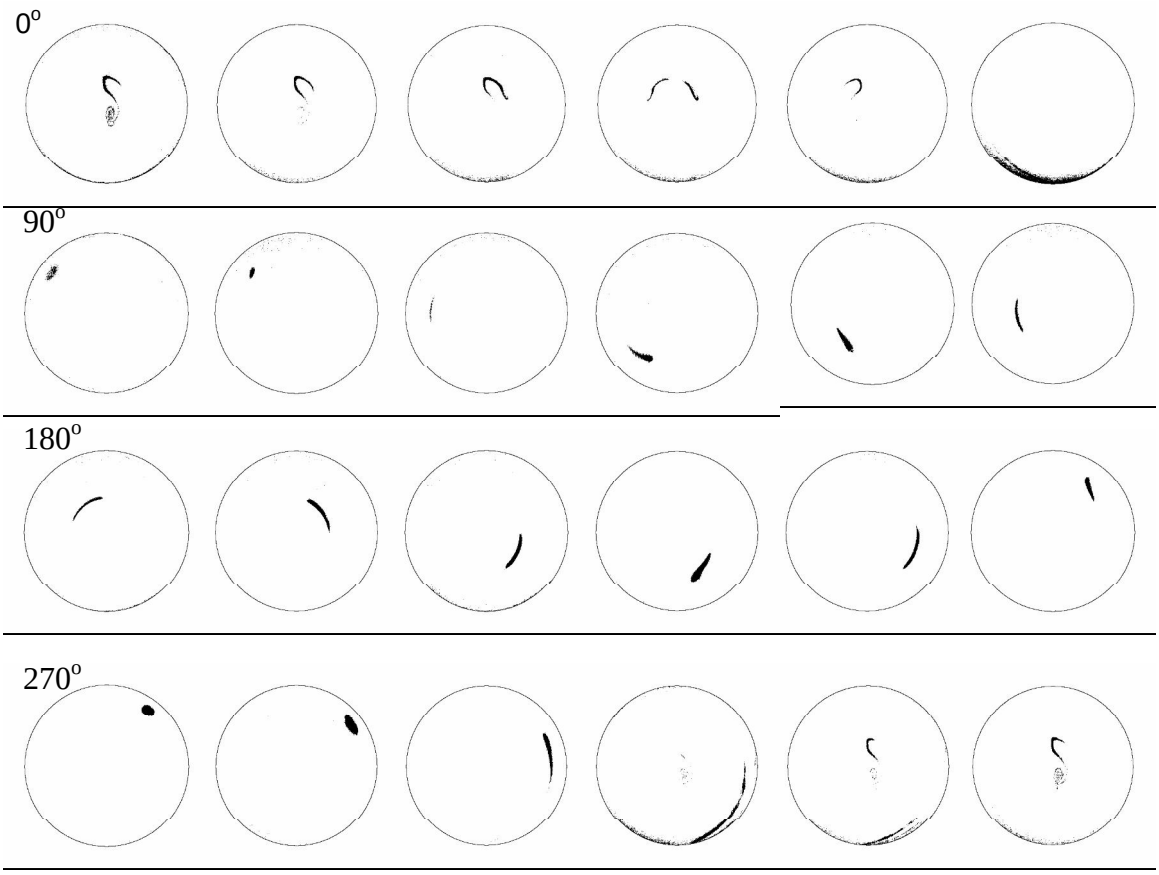

Figure 3-13: Resin oral airway exit, flow of 2 SLPM through 40% offset seed tube nozzle

Other than the odd seed stream shape in the 315° through 75° there is a pattern that the seed stream follows. Beginning in the anterior-right quadrant along the edge in the 90° case, the particles move in a counter-clockwise direction along the edge. In case 150° the seed stream moves in towards the center slightly and begins a clockwise path until the 240° cases where the particle stream moves out towards the edge. Then it moves counter-clockwise again along the edge.

3.5.1.1 Comparison of Glass and Resin Oral Airway Results

When the experiments were completed using the resin oral airway, it was imperative that results from it be compared to previous results from the glass model. The results from the two different models are not similar. This could possibly be the result of the surface properties of the two different materials. However, it is most likely due to the uncertainty of the geometry of the glass oral airway model.

3.5.2. Sodium Chloride Particles Generated by Nebulizer

The experiments performed using the nebulizer yielded very clear images. This was due to the high concentration of seeding material in the flow. All of these experiments had a bulk flow rate of 2 SLPM and a seed flow rate of 20 SCCM. Due to the high concentration of seed material in the flow, the amount of time the filters were exposed to the seeded flow, also referred to as run time, for each oral airway experiment needed only to be one minute. For the three generation bifurcation experiments the run time was lengthened to 8 minutes. Figure 3-14, Figure 3-15, and Figure 3-16 show the full set of both the oral airway results and the three generation bronchial bifurcation results of flow seeded with NaCl particles from the nebulizer. Once again the nozzle with the 40% offset seed tube was used.

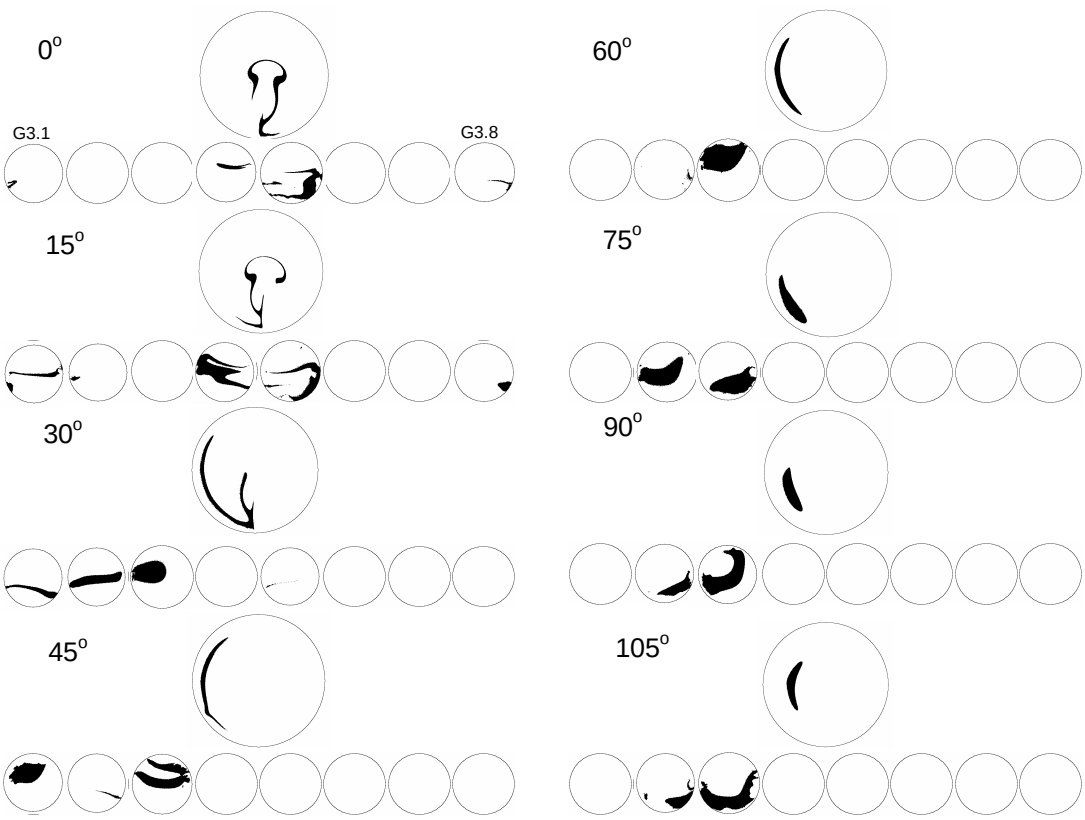

Figure 3-14: Oral airway and three generation bronchial bifurcation results (0^o-105^o)

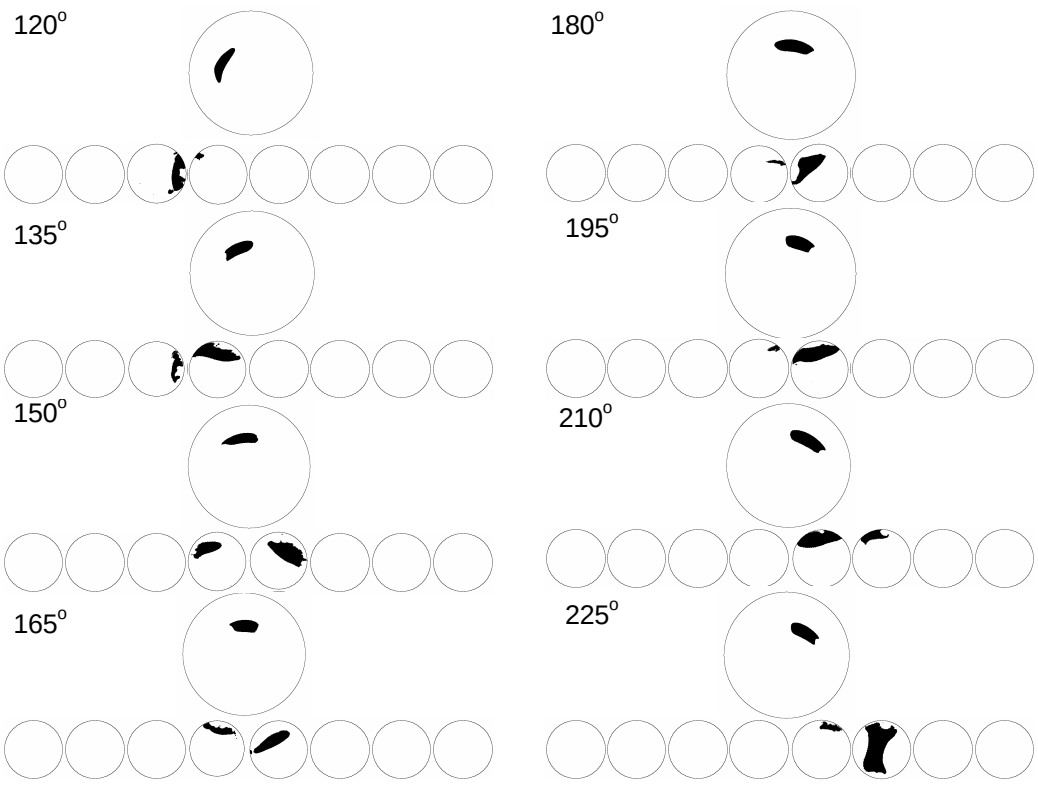

Figure 3-15: Oral airway and third generation results (120°-225°)

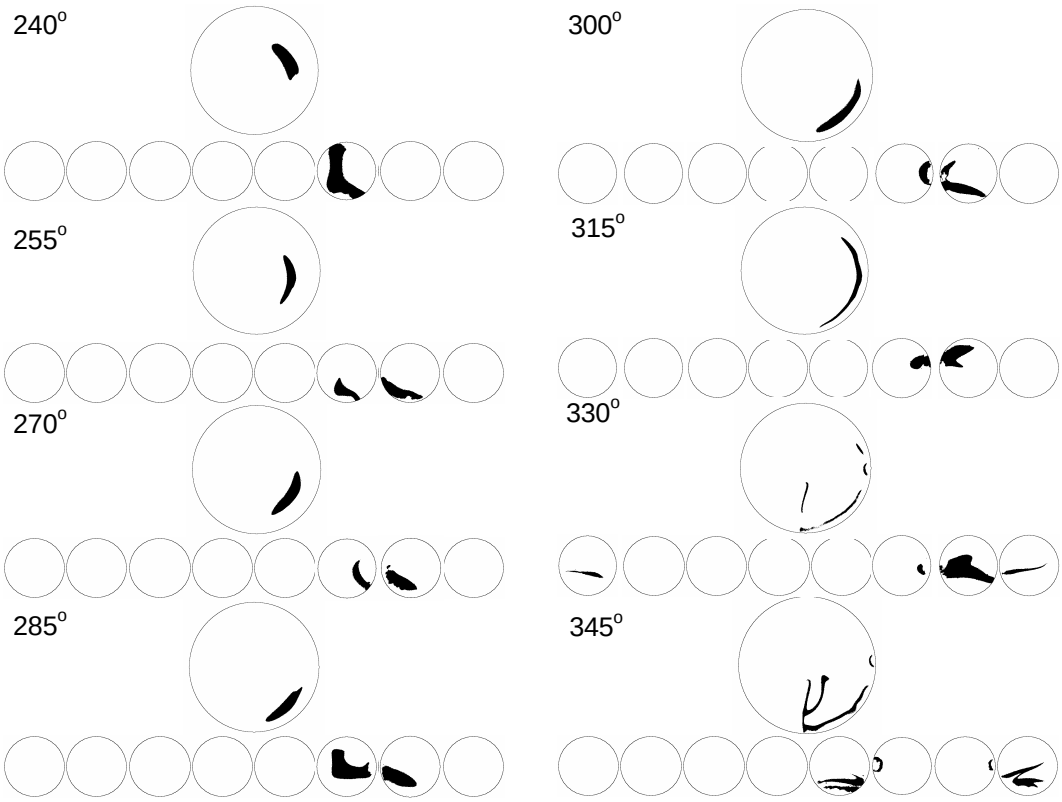

Figure 3-16: Oral airway and third generation results (240°-345°)

Similar to the resin oral airway results with the incense, the seed stream follows a path in the exit of the oral airway with NaCl as the seed medium. Beginning in the 45° case, the particles are close to the left edge. The particles then move in a counter-clockwise direction remaining along the edge until the 90° case when the seed stream moves slightly in towards the middle. From 105° to 270° the seed stream gradually moves in a clockwise direction. At 285° the seed stream then migrates outward towards the edge and in 300° and 315° the stream moves counter-clockwise again. The cases of 330° through 30° result in the appearance and dissipation of an odd mushroom-cloud shape. These

particle injection locations relate to the roof of the mouth. The seeded flow must follow a path along the outside of the curve possibly resulting in impaction with the wall at the soft palate or the glottis.

When the results of the experiments performed with the three generation bifurcation are arranged together it is visible to see the "path" followed as the particle injection location is rotated around the entrance to the test section (Figure 3-17).

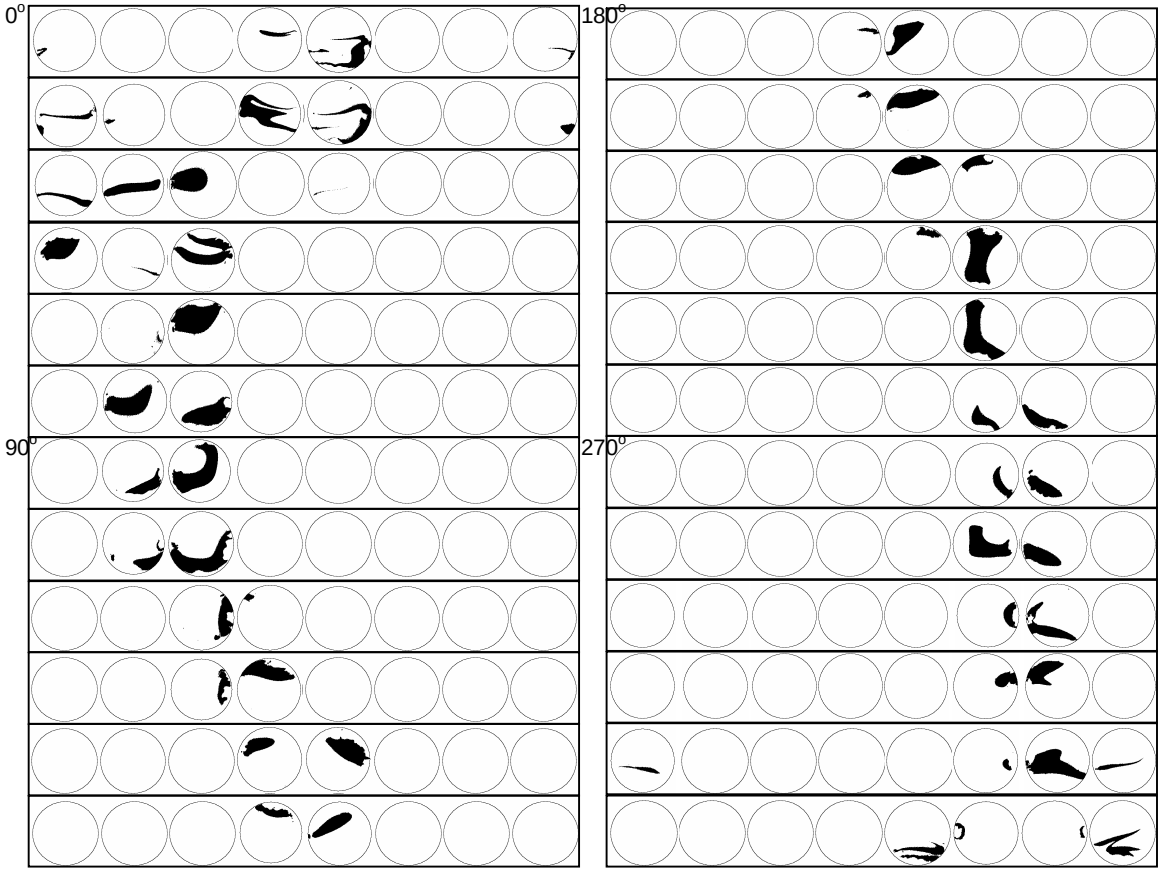

Figure 3-17: Resin three generation bronchial bifurcation results using the 40% offset seed tube nozzle, a 2 SLPM flow rate and NaCl particles

The control of the particles, to the extent of the seed stream exiting only one of the eight branches is desired. This only occurs in the 240^{o} case. Controlling to two adjacent branches in 18 out of 24 cases is a good start. A handful of cases have a majority of the seed stream in one branch and only a small amount of particles in an adjacent branch. Based on these results it is fully expected that an angle could be found where all the particles exit from a single branch.

3.5.3. Sodium Chloride Particles Generated by VOAG

Experiments were run with the VOAG with the assumption that it was producing 7 μm particles. The particles were actually 0.8 μm. This explained the reasons behind the similarities with the 1 μm particles from the nebulizer. The run time for experiments with the VOAG is very lengthy due to the low concentration of seed particles in the flow. The oral airway tests need a minimum of a 20 minute run time and the seed is still barely visible on the filters. The three generation experiments require an even longer run time. The results in Figure 7-12 and Figure 7-13 are from tests with a 20 minute run time for the oral airway and a one hour run time for the three generation bronchial airway. These tests were also run with a 2 SLPM bulk flow rate and a 20 SCCM seed flow rate. The flow enters the test section through the nozzle with the 40% offset seed tube.

3.6. Comparison of Computational and Experimental Results

The aim of this research was to validate the computational models used for particle deposition studies. Figure 3-18 shows the experimental and computational

results for a selection of cases. The computational results are presented in one image with the cases color-coded.

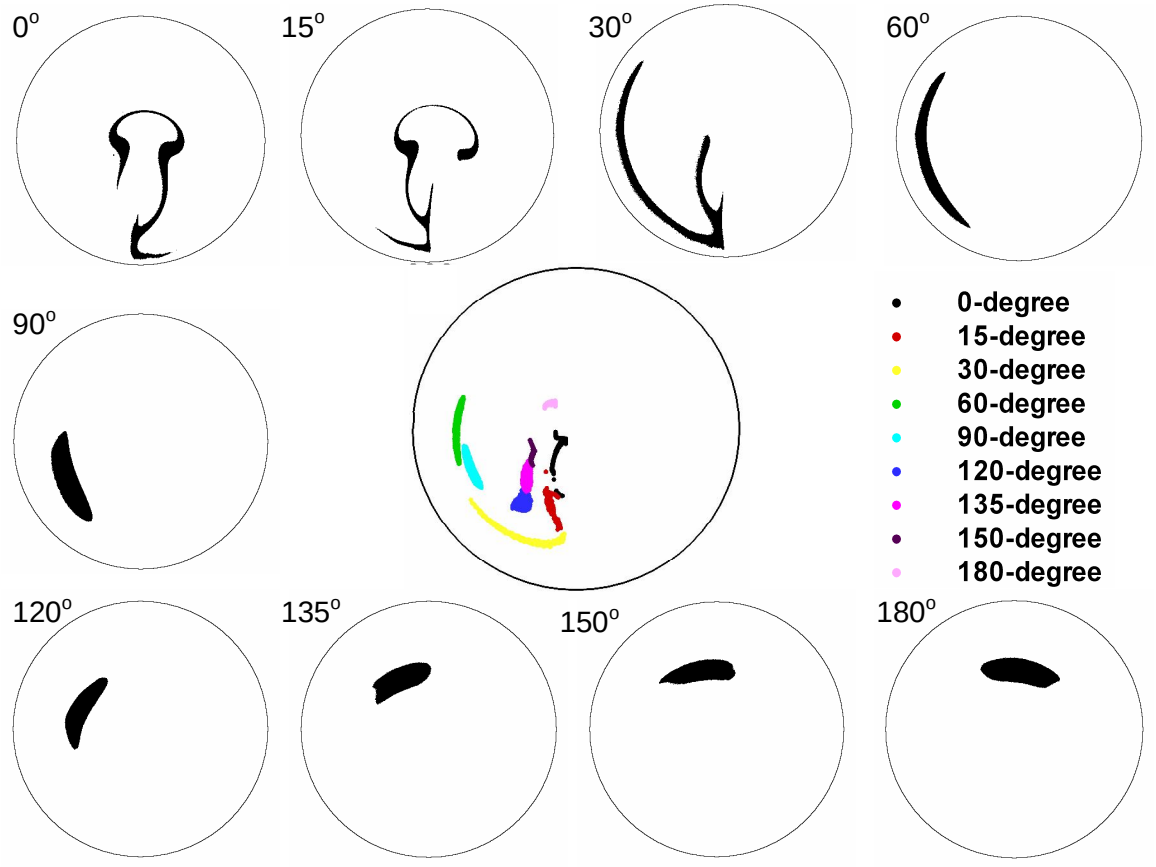

Figure 3-18: Comparison of experimental and computational results for 1 μm particles

Several cases agree in some way. The 90° case yields the best results. For the cases of 0° through 60°, the location of the seed stream of the computational results is contained within the seed stream of the experimental results. There is not much similarity in the 120° through 180° cases.

4.0 Conclusions

Once the flow rates were successfully controlled and an acceptable seeding method was established, deterministic control of the particle stream through the complex geometry of the human airway model was achieved. The extent of control is revealed in the results from the three generation bronchial bifurcation. The use of only one of the radially offset seed injection cases (40% offset nozzle), injecting at 15 degree increments only represents a fraction of the possible seed tube positions. Even with these limited results, the seed stream can be forced through each of the eight branches in the three generation model. The particle transport path can be predicted to just two branches in a majority of the cases and through a single branch in one case. The difficulty still remains in getting a majority of the particles to reach either of the outer branches. The one micrometer particles generated form the nebulizer yielded good results, however if the goal is to mimic aerosol drug characteristics larger particle will need to be used.

5.0 Future Work

Whereas, many aspects of his research were investigated, there is much experimentation remaining.

5.1. Other Nozzles

There are currently five stationary seed tube nozzles that have been constructed and are ready for use in experiments. Three of them have not been used with the most recent seeding method. There are doubts about the construction of the 80% nozzle the seed tube may be to close to the edge causing interruptions in the flow. The nozzles with the seed tube offset at 60% and 20% of the radius seem to be ready to go through the same experiments as the 40% offset nozzle has done.

Currently, there is a nozzle being designed that will have a movable seed tube, eliminating the need for a series of nozzles with stationary seed tubes. Once this nozzle is completed research should be conducted with it.

5.2. Particles

Although much experimentation has been done to try and find an ideal seeding material an method, one has not been found yet. There are a number of ideas, some branching off of methods and material already used, some employing all new methods and materials. One idea is to use the CMAG with oil that fluoresces. Along the same lines, the use of the CMAG as is should be reinvestigated. Now that the image acquisition utilizes a more powerful light source there is a possibility the fluorescence

will be activated enough even through the layer of oil. Even though the CMAG is capable of producing monodisperse oil droplets in the desirable size range there is still deviations. The idea of using PSL microspheres has been discussed. The size of these is known and unalterable. The can be aerosolized using a simple nebulizer. The disadvantage of using these is the cost. Another option is a powder dispersers, in which the seed material has a known size and is monodisperse. This option also has the disadvantage of being costly. A powder disperser would have to be purchased and a good material needs to be investigated and could be very costly.

5.3. Transient Flow

All the current research has been conducted using a constant flow rate. A more realistic transient breathing pattern should be used for experiments in the future. A mechanism has already been designed and built for this endeavor.

5.4. Further Generations of Bifurcations

The latest experiments have used the resin oral airway with and without the third generation bifurcation. Additional experiments need to be run with the current three generation model, but a model containing more generations has been considered.

5.5. Asymmetric Bifurcations

There is still much testing that can be done with the asymmetric bifurcations. Testing with this model and one containing further generation is important in order to get an accurate representation of the flow through a realistic human airway model.

6.0 References

Berglund, RN and Liu, BYH. Generation of monodisperse aerosol standards, *Environmental Science and Technology* 7 (1973), pp. 147-153.

Cheng, Y.S., Bechtold, W.E., Yu, C.C., and Hung, I.F. (1995). Incense smoke: characterization and dynamics in indoor environments, *Aerosol Science and Technology*, 23, 271-281.

Cheng, Y. S., Zhou, Y., & Chen, B. T. (1999). Particle deposition in a cast of human oral airways. *Aerosol Sci. Technol., 31*, 286-300.

Crowder, T. M., Lousy, M. D., Sethuraman, V. V., Smyth, H. D. C., and Hickey, A. J. (2001). An Odyssey in Inhaler Formulation and Design, *Pharmaceutical Technology*, July 2001:99-113.

Dunbar, C. A., Hickey, A. J., and Holzner, P. (1998). Dispersion and Characterization of Pharmaceutical dry Powder Aerosols, *KONA* 16:7-44.

Finlay, W.H. (2001). *The Mechanics of Inhaled Pharmaceutical Aerosols: An Introduction*. London, UK: Academic Press.

Jetter, J.J, Guo, Z., McBrian, J.A., and Flynn, M.R. (2001). Characterization fo emissions from burning incense. *Science of the Total Environment*, 295, 51-67.

Kim, C.S. & Fisher, D.M. (1999). Deposition of aerosol particles in successively bifurcating airways models. *Aerosol Science and Technology 31***,** 198-220.

Kleinstreuer, C. (2003). *Two-Phase Flow: Theory and Applications*. Taylor & Francis, New York.

Kleinstreuer, C., & Zhang, Z. (2003a). Laminar-to-turbulent fluid-particle flows in a human airway model. *Int. J. Multiphase Flow, 29*, 271-289.

Kleinstreuer, C., and Zhang, Z. (2003b). Targeted drug aerosol deposition analysis for a four-generation lung airway model with hemispherical tumors, *ASME Journal of Biomechanical Engineering*, 125(2), 197-206.

Oulu University - http://herkules.oulu.fi/isbn9514252217/html/x317.html

Weibel, E. R. (1963). *Morphometry of the Human Lung*. New York: Academic Press.

Zhang, Z., Kleinstreuer, C & Donohue, J.F. (2003b). Comparison of micro- and nano-size particle depositions in a human upper airway model, *Journal of Aerosol Science*, Submitted for publication.

Z. Zhang and C. Kleinstreuer, Airflow structures and nano-particle deposition in a human upper airway model, *Journal of Computational Physics* **198** (2004), pp. 178–210.

7.0 Appendices

7.1. Appendix A – SmartMotor Linear Actuator Data

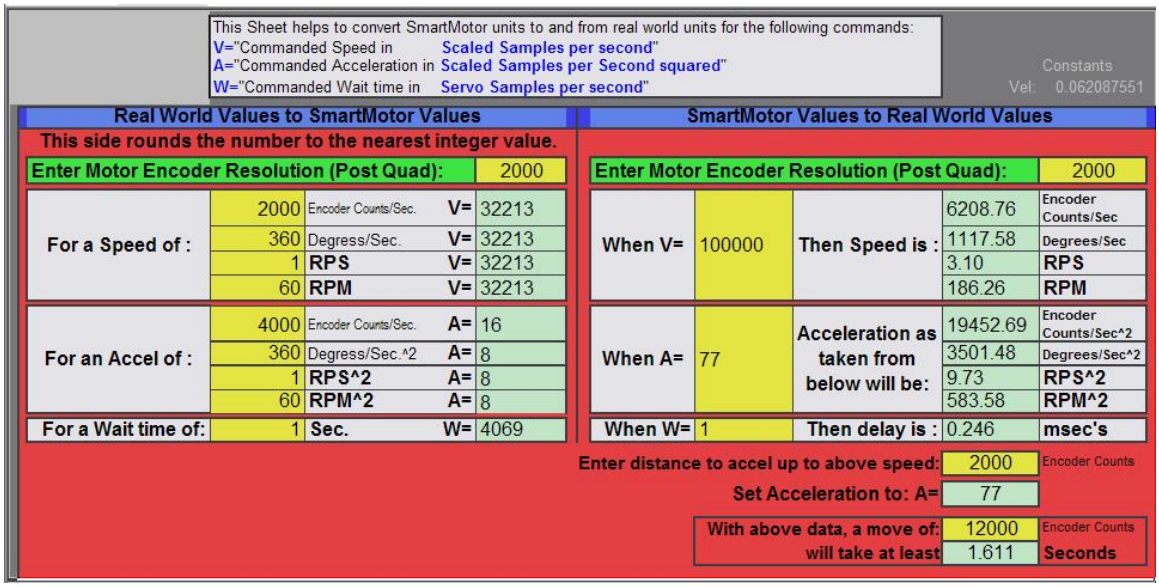

This Sheet helps to convert SmartMotor units to and from real world units for the following commands:
V="Commanded Speed in Scaled Samples per second"
A="Commanded Acceleration in Scaled Samples per Second squared"
W="Commanded Wait time in Servo Samples per second"

Constants
Vel: 0.062087551

Real World Values to SmartMotor Values

This side rounds the number to the nearest integer value.

Enter Motor Encoder Resolution (Post Quad):				2000
For a Speed of :	2000	Encoder Counts/Sec.	V=	32213
	360	Degress/Sec.	V=	32213
	1	RPS	V=	32213
	60	RPM	V=	32213
For an Accel of :	4000	Encoder Counts/Sec.	A=	16
	360	Degress/Sec.^2	A=	8
	1	RPS^2	A=	8
	60	RPM^2	A=	8
For a Wait time of:	1	Sec.	W=	4069

SmartMotor Values to Real World Values

Enter Motor Encoder Resolution (Post Quad):				2000
When V=	100000	Then Speed is :	6208.76	Encoder Counts/Sec
			1117.58	Degrees/Sec
			3.10	RPS
			186.26	RPM
When A=	77	Acceleration as taken from below will be:	19452.69	Encoder Counts/Sec^2
			3501.48	Degrees/Sec^2
			9.73	RPS^2
			583.58	RPM^2
When W=	1	Then delay is :	0.246	msec's

Enter distance to accel up to above speed: 2000 Encoder Counts

Set Acceleration to: A= 77

With above data, a move of: 12000 Encoder Counts

will take at least 1.611 Seconds

Figure 7-1: Example of a worksheet design to convert SmartMotor values to real world values and vice versa

Table 7-1: Input values for one cycle of breath with 680 ml/s maximum and constant inlet flow rate of 340 mL/s

1	Time (s)	Inlet Flow Rate (mL/s)	Inlet Flow Rate (mL/s)	Speed of Actuator (cm/s)	Required Velocity (Counts/s)	Encoded Velocity (V=)	Distance (counts)	Position (counts)
2	0	0	-340	-0.9319	-17611	-283655	-22692	-22692
3	0.04	65	-275	-0.7538	-14245	-229427	-18354	-18354
4	0.08	130	-210	-0.5756	-10878	-175199	-14016	-14016
5	0.12	195	-145	-0.3974	-7511	-120971	-9678	-9678
6	0.16	260	-80	-0.2193	-4144	-66742	-5339	-5339
7	0.2	311	-29	-0.0808	-1527	-24593	-1967	-1967
8	0.24	361	21	0.0577	1090	17560	1405	1405
9	0.28	412	72	0.1962	3707	59713	4180	4180
10	0.32	462	122	0.3347	6325	101866	13243	13243
11	0.35	500	160	0.4386	8288	133485	26697	26697
12	0.45	565	225	0.6167	11655	187713	37543	37543
13	0.55	610	270	0.7401	13986	225256	45051	45051
14	0.65	640	300	0.8223	15540	250284	50057	50057
15	0.75	660	320	0.8771	16576	266970	53394	53394
16	0.85	665	325	0.8908	16835	271141	54228	54228
17	0.95	670	330	0.9045	17093	275313	55063	55063
18	1.05	670	330	0.9045	17093	275313	55063	55063
19	1.15	665	325	0.8908	16835	271141	54228	54228
20	1.25	660	320	0.8771	16576	266970	53394	53394
21	1.35	640	300	0.8223	15540	250284	37543	37543
22	1.45	605	265	0.7264	13727	221084	15476	15476
23	1.5	540	200	0.5482	10360	166856	10011	10011
24	1.52	500	160	0.4386	8288	133485	10679	10679
25	1.56	447	107	0.2922	5523	88947	7116	7116
26	1.6	393	53	0.1460	2760	44452	3556	3556
27	1.64	340	0	-0.0001	-3	-43	-3	-3
28	1.68	287	-53	-0.1463	-2765	-44538	-1782	-1782
29	1.7	260	-80	-0.2193	-4144	-66742	-4005	-4005
30	1.72	208	-132	-0.3618	-6837	-110125	-8810	-8810
31	1.76	104	-236	-0.6469	-12224	-196890	346527	346527
32	1.8	0	-340	-0.9319	-17611	-283655	510580	510580

7.2. Appendix B – Chart of Results

Table 7-2: Summary of experiments performed in this research

	Hollow Glass Spheres	Diesel Smoke	Incense	NaCl Particles
Straight Tubes	Simple tests using light activity flow rates. Used to determine the spray angle, if any, of the seeded flow		Used to test the effects of a non-velocity-matched set of flows. The 20 cm straight tube was used with an constant bulk flow rate and varying seed flow rates. Also some experiments to test the effect of length on the flow.	
Long Bend	Simple tests using light activity flow rates. Used to determine the effects of a simple bend on the flow. Also performed limited experiments testing the effect of seed flow rates higher than the velocity matched flows	Limited tests using bulk flow that yielded a Reynolds number of 2000.	Simple tests to compare to the straight tube results.	
Glass Oral Airway	One experiment with very poor results.	Used to test for the highest flow rate that could be used and still remain in the laminar flow regime. Simple experiments performed to show the effects of the change in seed injection location on the flow	Full set of experiments performed using the 2 SLPM flow rate and 40% nozzle in 15 degree increments.	
Glass First Generation Symmetric Bifurcation			Full set of experiments performed using the 2 SLPM flow rate and 40% nozzle in 15 degree increments.	
Glass First Generation Asymmetric Bifurcation			Full set of experiments performed using the 2 SLPM flow rate and 40% nozzle in 15 degree increments.	
Glass Second Generation Bifurcation			Set of experiments performed using the 2 SLPM flow rate and 40% nozzle in 15 degree increments yeilding only results for the right most branch (G2.4).	
Glass Third Generation Bifurcation				
Resin Oral Airway			Full set of experiments performed using the 2 SLPM flow rate and 40% nozzle in 15 degree increments. Experiments repeated multiple times and results are consistent. Also compared to results from glass oral airway.	Full set of experiments performed using the 2 SLPM flow rate and 0% and 40% nozzle in 15 degree increments.
Resin Third Generation Bifurcation				Full set of experiments performed using the 2 SLPM flow rate and 0% and 40% nozzle in 15 degree increments.

7.3. Appendix C - Straight Tubes and Bends

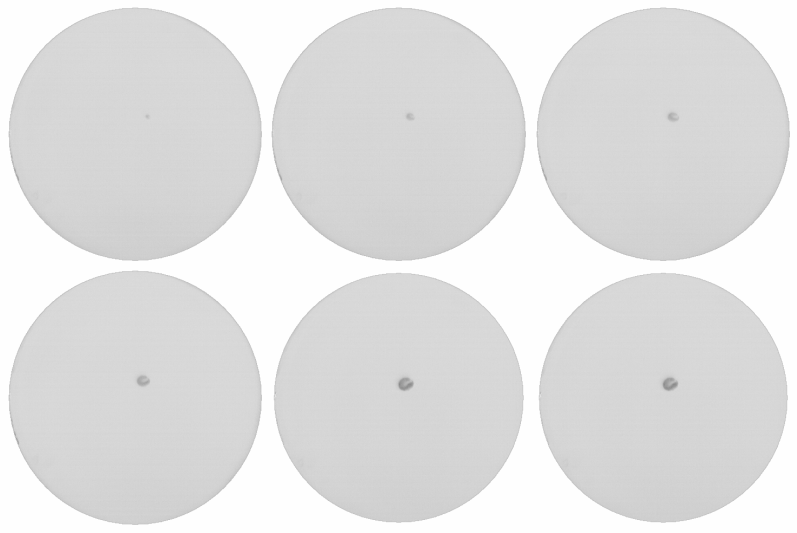

Figure 7-2: 0% nozzle velocity matching results: 5, 15, 25, 35, 45, and 55 SCCM (from top left across the rows), using incense as seeding medium

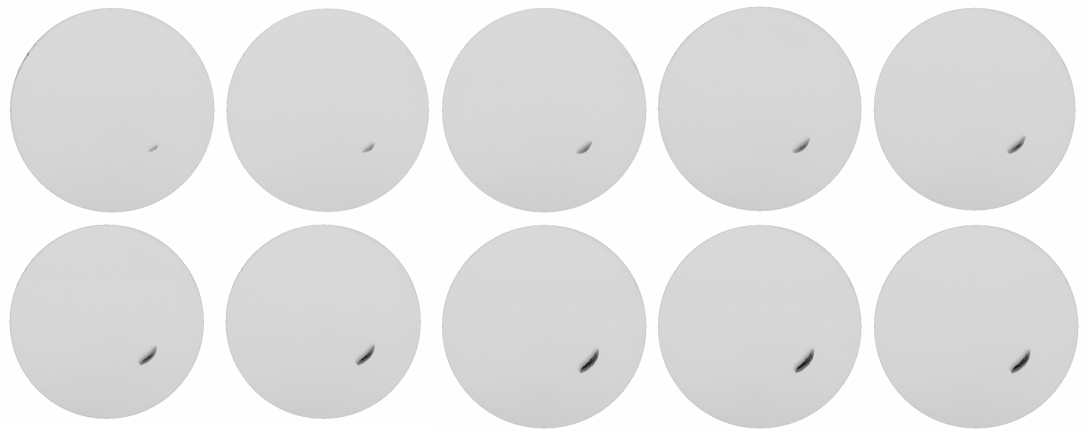

Figure 7-3: 20% nozzle velocity matching results: 5, 10, 15, 20, 25, 30, 35, 40, 45, and 50 SCCM seed flow rate (from top left across the rows) , using incense as seeding medium

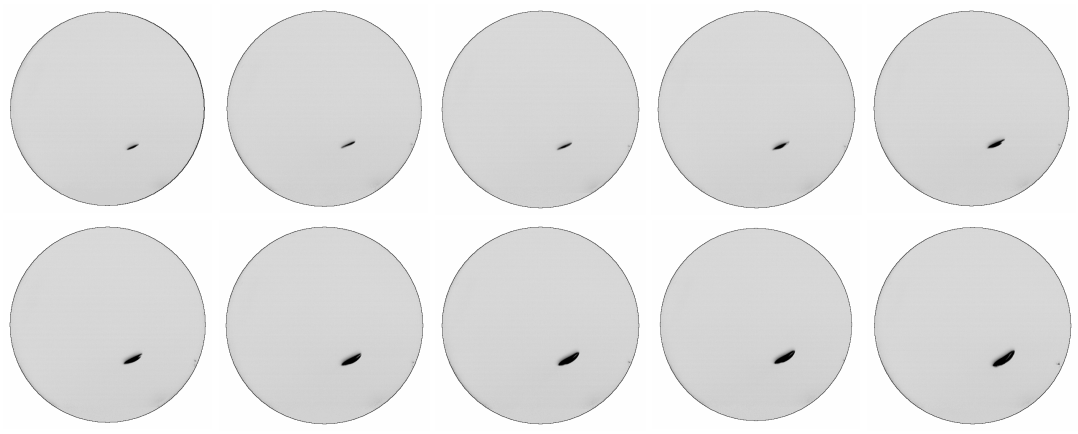

Figure 7-4: 40% nozzle velocity matching results: 5, 10, 15, 20, 25, 30, 35, 40, 45, and 50 SCCM seed flow rate (from top left across the rows) , using incense as seeding medium

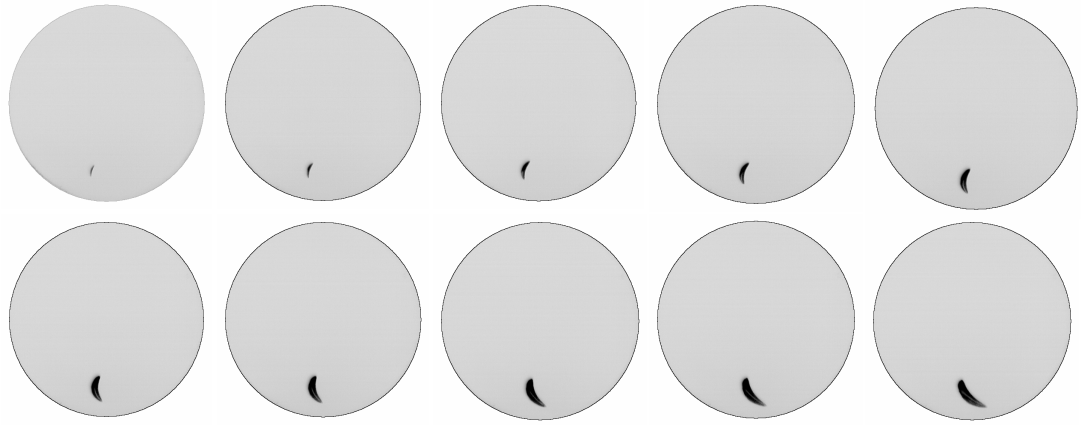

Figure 7-5: 60% nozzle velocity matching results: 5, 10, 15, 20, 25, 30, 35, 40, 45, and 50 SCCM seed flow rate (from top left across the rows) , using incense as seeding medium

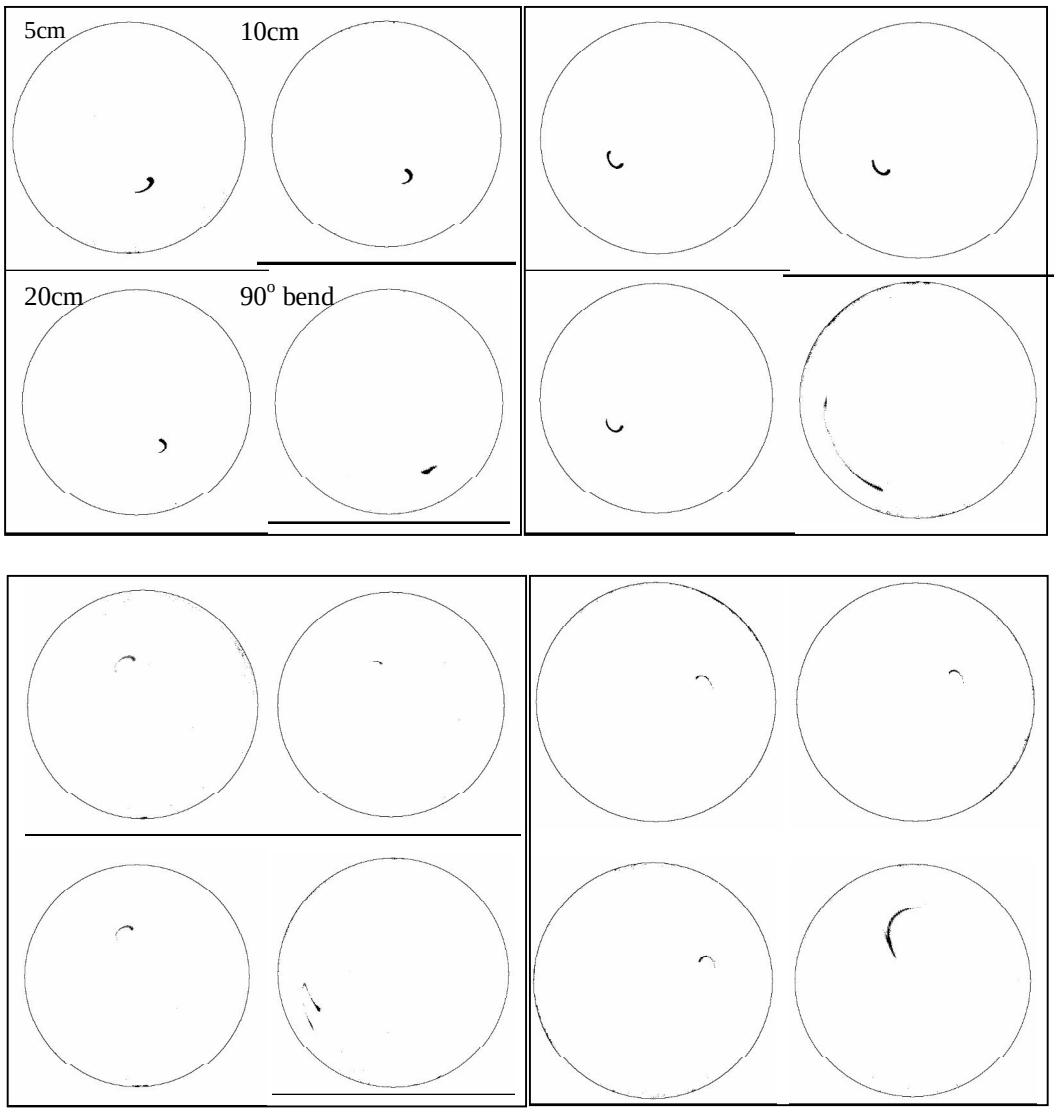

Figure 7-6: Results from straight tubes and bends using incense each set of four images contains one of each: 5 cm straight tube, 10 cm, 20 cm, and 90 degree bend

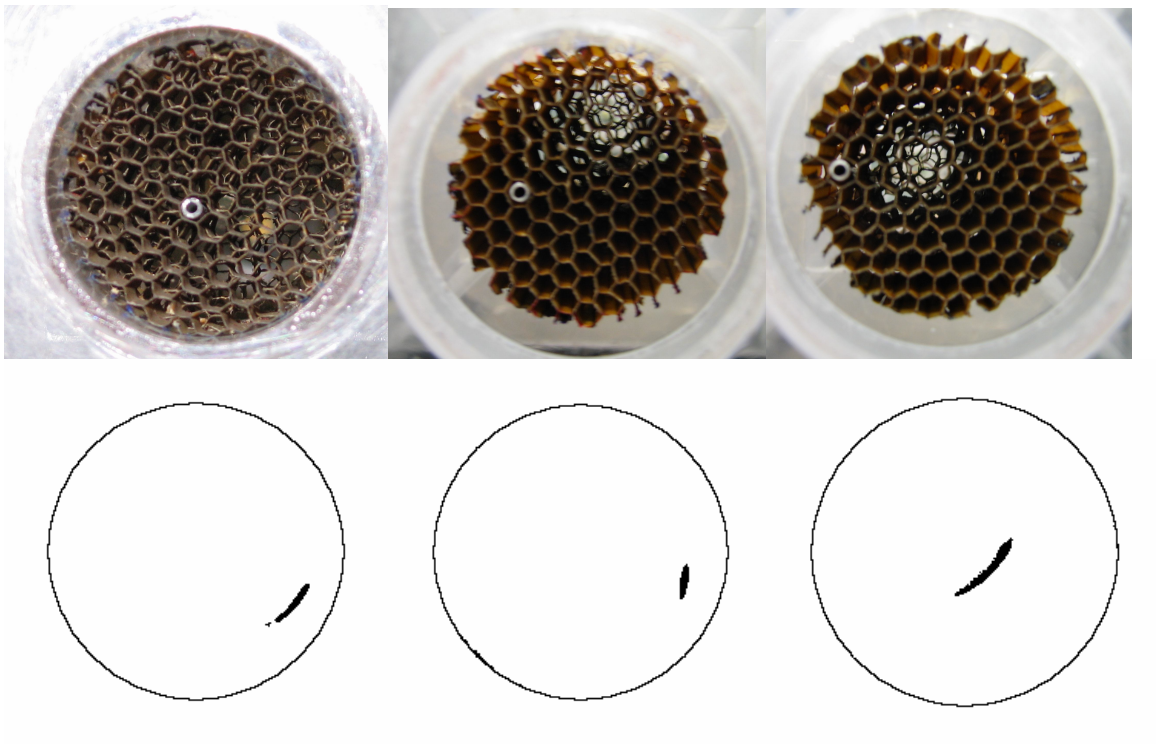

Figure 7-7: Results from three seed exit locations using diesel smoke, through the 90^{o} bend

7.4. Appendix C – Glass Oral Airway and Bifurcations

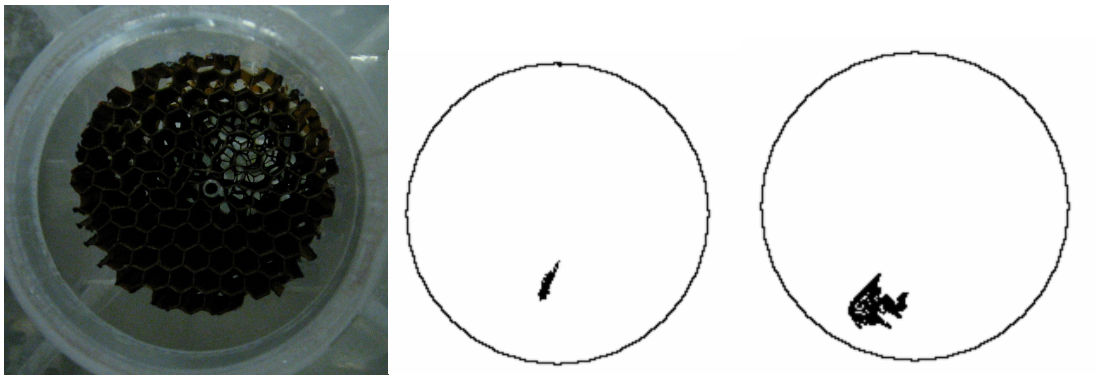

Figure 7-8: Seed injection location and results from oral airway using diesel smoke, seed injection location in the center, 8 SLPM flow rate, 12 SLPM flow rate

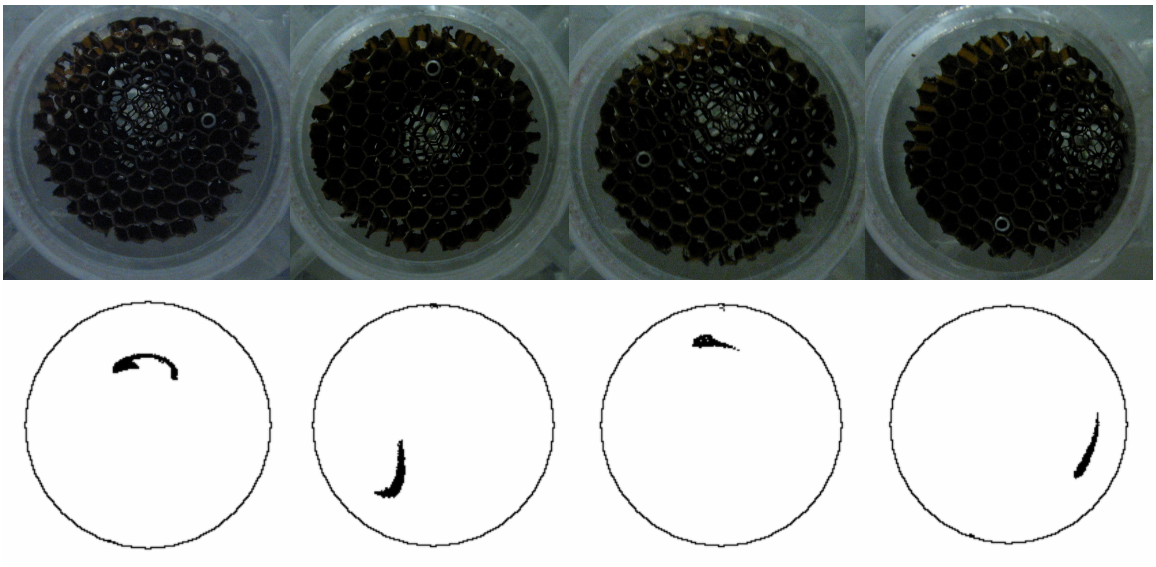

Figure 7-9: Seed injection locations and results from oral airway using diesel smoke a) right, b) top, c) left, and d) bottom

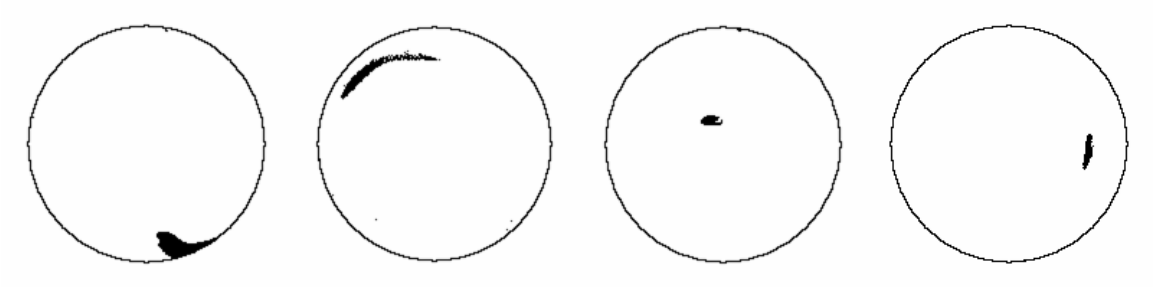

Figure 7-10: Incense result using the glass oral airway for a) 0^o, b) 90^o, c) 180^o, d) 270^o

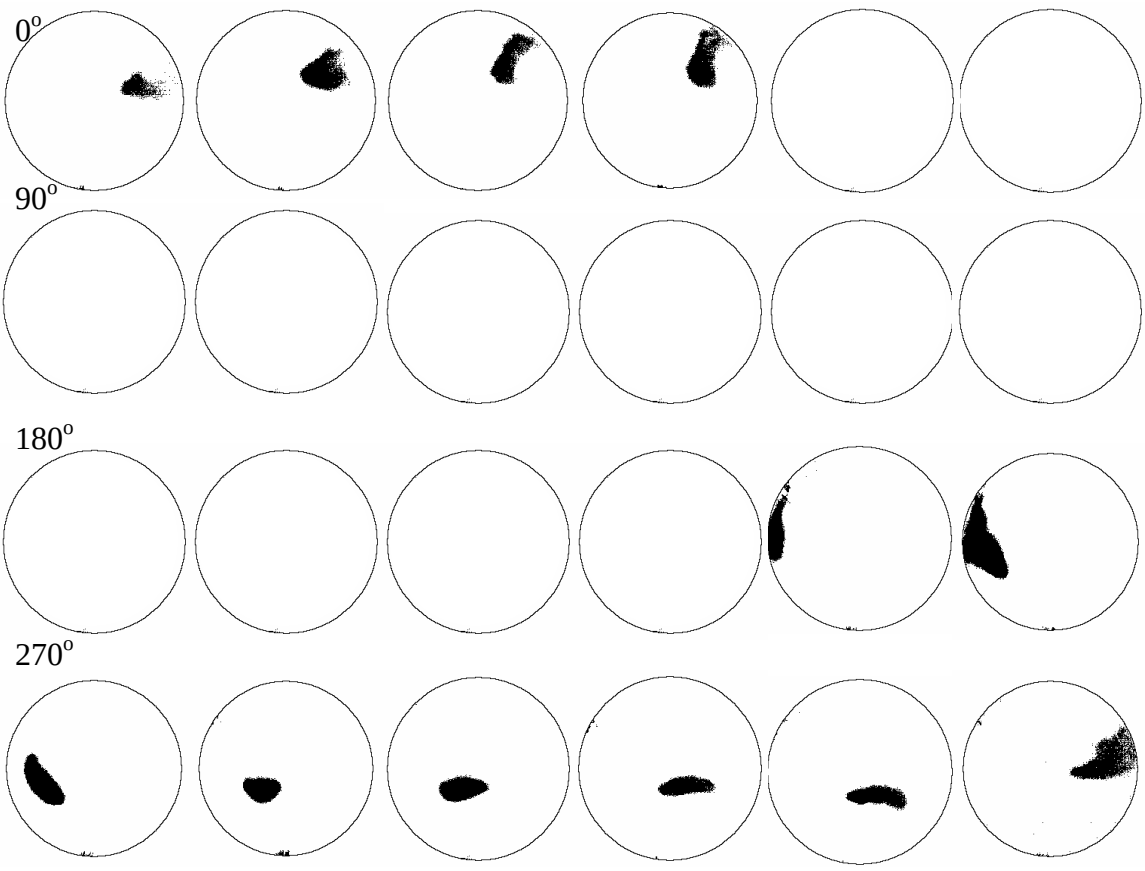

Figure 7-11: Right most second generation bifurcation exit (G2.4), full set of 360^o in 15^o increments from left to right, using incense as seeding medium

7.5. Appendix D – Resin Oral Airway and Bifurcations

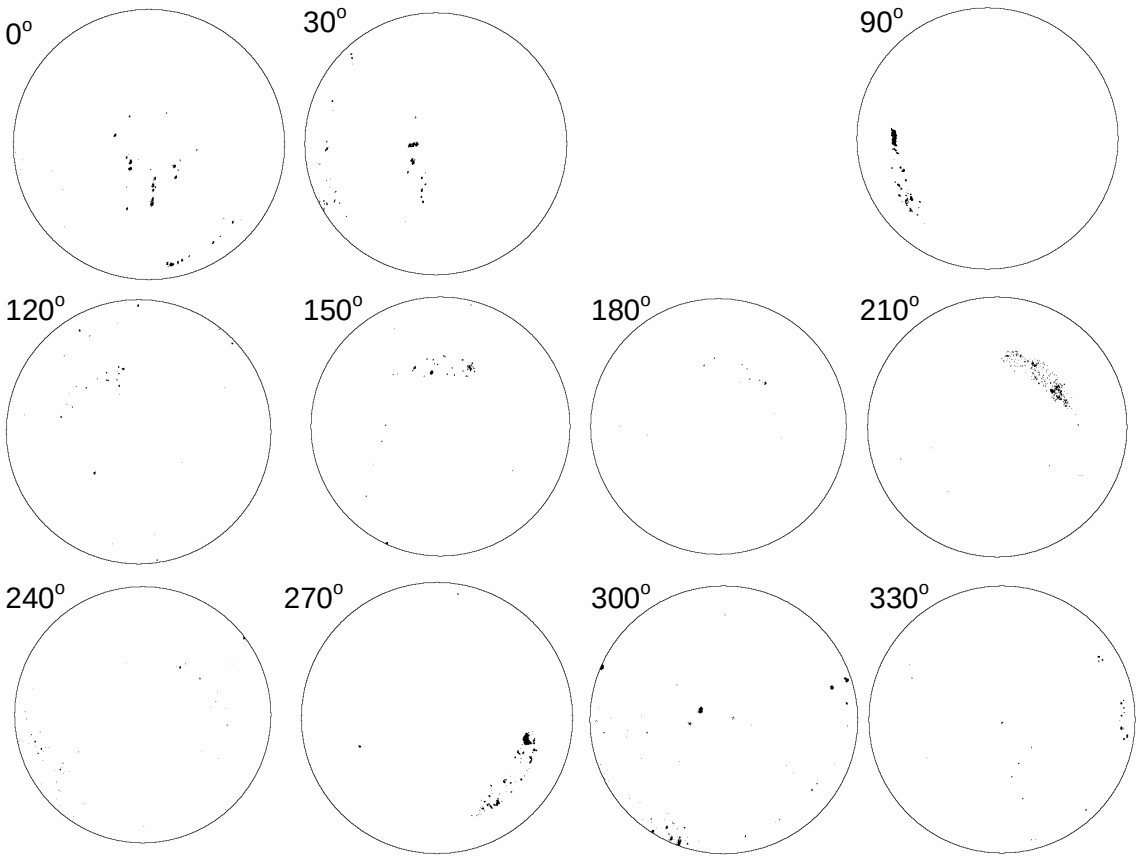

Figure 7-12: Resin oral airway results with VOAG, actual particle size roughly 0.8 µm

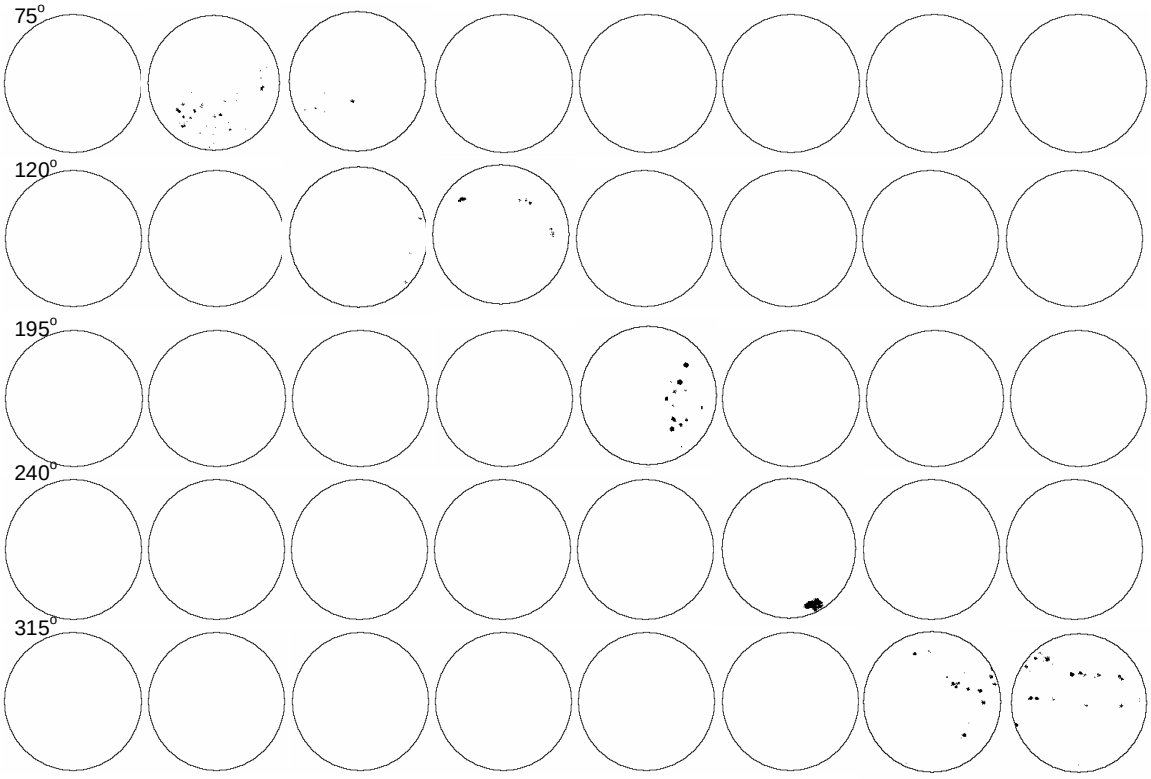

Figure 7-13: Resin three generation bifurcation results with VOAG